remote sensing

MDPI

Article

Development of Geospatial and Temporal Characteristics for Hispaniola's Lake Azuei and Enriquillo Using Landsat Imagery

Mahrokh Moknatian [1], Michael Piasecki [1,*] and Jorge Gonzalez [2]

[1] Civil Engineering Department, City College of New York, New York, NY 10031, USA; mmoknat00@citymail.cuny.edu

[2] Mechanical Engineering Department, City College of New York, New York, NY 10031, USA; jgonzalezcruz@ccny.cuny.edu

* Correspondence: michael.piasecki@gmail.com or mpiasecki@ccny.cuny.edu; Tel.: +1-610-564-8184

Academic Editors: Magaly Koch and Prasad Thenkabail
Received: 11 February 2017; Accepted: 14 May 2017; Published: 24 May 2017

Abstract: In this paper, we used Landsat imagery for water body identification to create a novel 36-year surface area extent time series for lakes Azuei (Haiti) and Enriquillo (Dominican Republic) aimed at illuminating the dramatic temporal changes of these two lakes not just at yearly but at monthly or even sub-monthly scales. We used the Normalized Difference Water Index (NDWI) to extract water features and we also used spatial differentiation and thresholding techniques to remove clouds and associated shadows from the scene that were then passed through gap filling algorithms to complete and extract the lake extent polygons. We also explored the challenges that arrive from trying to combine RS-based Digital Elevation Model data with locally collected bathymetric data to yield a seamless representation of the topographic features of the rift valley that contains the two lakes. This "bathtub" model was then meshed with the lake extent polygons to compute lake volumes, maximum depths, and geospatially referenced lake levels rating curves. We used this data to examine the lakes and their geospatial characteristics in the context of the lakes' growth/shrinking patterns. While we did not carry out a full hydrologic analysis we attempted to illuminate how specific lake levels cause what type of flooding and especially answered the questions if (a) Lake Azuei would ever spill into Lake Enriquillo, and (b) what the maximum lake levels need to be before spilling into neighboring watersheds.

Keywords: remote sensing; lake; water dynamics; NDWI; cloud detection; shadow removal; gap filling; bathymetry; rating curve

1. Introduction

Remote sensing has opened the door for large-scale geospatial analyses of both geographic features and land/ocean surfaces. While there are numerous satellites orbiting the globe that have a multitude of instruments on-board that explore various bandwidths in the electro-magnetic spectrum, Landsat based images are ideally suited for surface feature analyses because of its high spatial resolution imagery. Hence, these images, in this study collected from Landsat satellites 4, 5, and 7 (the first, Landsat 1, was launched in 1972 while the latest, Landsat 8, in 2013) provide a "view" of the earth surface from 1984 to the present. Landsat images were and continue to be taken twice a month around 16 days apart thus providing us with an imagery pool of about 300 images between 1984 and 2014 (theoretically it could be about 480 but not all years have 2 images/month schedule). Note, that not all the images could be used since many of them contain clouds, cloud shadows, topographic shadows, and missing imagery data due to the failure of the ETM+ scan line corrector (SLC) on Landsat 7.

Despite these constraints, the temporal resolution adds to the suitability of using the scenes to track lake surface extents namely because the processes that drive lake surface area growth or decline are slow enough to be captured well with a 16-day repeat frequency. In this paper we outline a procedure to use this pool of about 300 images to create a Lake Surface Area time series of two lakes on the Island of Hispaniola in addition to some applications that are based on the generation of these time series.

The island of Hispaniola is home to two of the largest lakes in the Caribbean; Lake Azuei (or Etang Saumatre) on the Haitian side and Lake Enriquillo on the Dominican side both of which are located in the Hispaniolian rift valley and are just separated by a 2–3 mile wide peninsula along the border between these two countries; Figure 1. The lakes are endorheic in nature, i.e., they have no outlet to the sea, are fed by their surrounding watersheds, and feature no man-made withdrawal/discharge controls. Both lakes have experienced a dramatic growth over the past roughly 10 years to unprecedented levels that have caused vast flooding in the western and eastern regions of each lake, inundating farmland, threatening small towns (e.g., Boca de Cachon in the DR), and disrupting a key trade transit road connecting the two countries along the border town of Jimani (DR) [1–8].

Figure 1. The island of Hispaniola with an insert showing our study area featuring the two lakes.

While the lakes have experienced some form of oscillatory growth and decline patterns over time the dramatic growth trend starting in 2004 has been unprecedented. Not surprisingly, this phenomenon has attracted considerable attention not only from the two governments who face the need to deal with the adverse effects but also from the scientific community trying to (a) shed some light as to the "why" and "how", and (b) trying to predict what might happen in the future, especially in view of changing climate patterns [9–18].

A key aspect in understanding the growth patterns has been to assess and identify the lake area extent as well as the bathymetry (and thus depth) of the lakes, allowing volume changes to be computed over time. To know these volume changes is essential when trying to compute the water balance for the lakes and their surrounding watersheds and in turn is a fundamental step in

understanding the lakes' behavior. However, reports on lake levels and area extents are not consistent throughout the literature which actually focuses mostly on Lake Enriquillo with little to no information available for Lake Azuei. In 2003, Schubert [19] reported that Lake Enriquillo surface area and volume were 254 km^2 and 1.4 km^3 respectively for the year of 1983, and 222 km^2 and 0.76 km^3 in 1992. He also stated that lake elevation was 43.3 m below Mean Sea Level (MSL) while lake volume was 0.76 km^3, in 1999. Buck and Brenner [10] reported that in 2000 the Lake Enriquillo elevation was 46 m below MSL with a surface area of approximately 200 km^2. Wright et al. [13] on the other side reported a lake elevation for Enriquillo of 49 m below MSL for the same year with additional estimates for, 1984 (49 m below MSL), 1997 (51 m below MSL), 2004 (54 m below MSL). The Dominican Instituto Nacional de Recursos Hidraulicos (INDRHI) estimated that from the years of 2000 to 2012 Lake Enriquillo had risen by up to 6 m and grown to 320 km^2 [12]. Based on the data INDRHI presented, Logan et al. [12] calculated that Lake Enriquillo must have expanded by 1.5 km^3 from 2000 to 2012 and also estimated that in 2012 between the months of July to September 0.16 km^3 of water had been added to the lake resulting in a 0.5 m rise. Another report published by Mendez-Tejeda et al. [11] suggest that between the years of 1982 to 2000, the surface area of Lake Enriquillo had been reported to fluctuate between 195 km^2 and 332 km^2 while Lake Azuei ranged between 113 km^2 to 118 km^2. Based on a NASA report, Pichardo et al. [18] suggested that the surface area of Lake Enriquillo changed from 205.35 km^2 in 2000 to 311.58 km^2 in 2009. Sources for Lake Azuei are much less numerous making a comparison literally impossible.

Although the lakes' surface area, volume, and elevation values are reported in the literature, the comparison is quite challenging. The challenges arise from the fact that the sampling rate of data (mostly satellite imagery, Landsat) is infrequent sometimes only featuring a single image per year or less in any of the time series published. In this regard, the time horizon also differs vastly with no long-term historic record being available. Lastly, documentation of methods and procedures used to analyze Landsat satellite imagery and the subsequent computation of lake extents and vertical reference levels is often poorly if not at all documented. It is well known that both lakes fluctuate throughout the year and are able to respond to short-term events such as Hurricanes and tropical storms. The lack of accounting for and documenting lake behavior at sub-annual time scales is pervasive in all the literature we examined thus missing out on documenting seasonal and sometimes even monthly patterns.

We outline the algorithm we developed to process all available Landsat images; delineating water bodies, removing clouds and their associated shadows, topographic shadows and data gaps from the image and complete missing parts of the water body using reference images. We also present a set of "rating" curves that are designed to provide the relationships between surface area extent and volume, surface area extent and maximum depth and, as a result, maximum lake depth and volume. Lastly, we are able to showcase a predictive tool which emerges from "stitching" together the bathymetry data we collected [20] and the surrounding 30 m Digital Elevation Model data that form two (one for each of the lakes) "bath-tub" models that we can fill and drain to show potential future levels and associated inundation areas.

2. Materials and Methods

2.1. Study Area

The Hispaniola rift valley features two large lakes, Lake Azuei in Haiti and Lake Enriquillo in the Dominican Republic. Lake Enriquillo is located in the lowest part of the valley Neiba, about 31.5 m below sea level (EGM96), covering the area of about 347.3 km^2 (measured in March 2013), also being the Caribbean's largest lake and lowest point. Almost five kilometers apart from Lake Enriquillo to the west with a level of 23 m above the sea level (EGM96), lies Lake Azuei with an area of 154.5 km^2 (measured in July 2013) thus having about half the surface area of Lake Enriquillo. The associated watershed areas are 713 km^2 for Lake Azuei and 3062 km^2 for Lake Enriquillo making the Enriquillo

basin about four times as big as the Azuei watershed. Both lakes in the past have exhibited a constantly changing water level that despite the close proximity to each other has not always been synchronous. While the general trend development aligns, especially the dramatic growth over the past 10 years, there are many instances where one lake grows while the other subsides and vice versa. As a result, the lake level difference oscillates between 45 m and 60 m throughout the years.

Both lakes lie in close proximity to the Enriquillo-Plantain-Garden fault that runs underneath the rift valley in east-westerly directions. The lakes are flanked to the north and south by high rise mountains while the eastern and western ends are flat and follow the general direction of the rift valley. The climate also varies from arid in the lowlands to very humid in the mountains especially at the Montane Forrest belt [21]. All the rivers and streams around both lakes are of ephemeral nature and each lake is approximately located in the center of their respective watersheds with no surface outlet to the sea, i.e., they are endorheic basins. Basins of this type are known to be very sensitive to slight changes in hydrological balance, which in turn, may cause significant changes in the water budget of the lake [22]. Figure 2 shows the two lakes, their associated watersheds, and color coded lake surfaces that contrast the extent in 2003 and 2014.

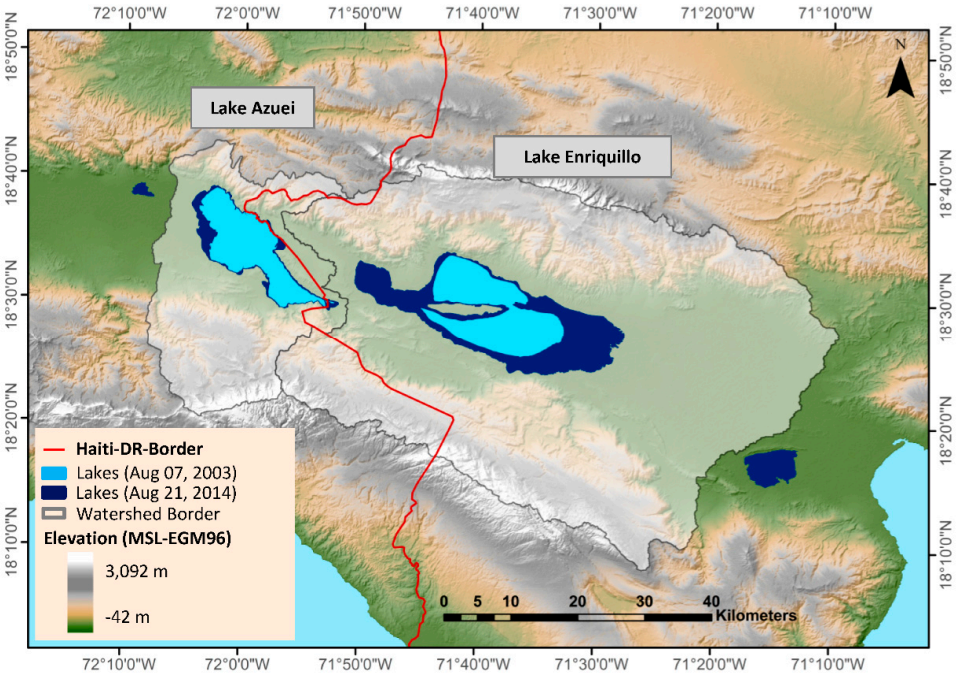

Figure 2. Study Area (lakes' extent is obtained using Landsat images).

2.2. Landsat Imagery Acquisition and Preprocessing

Our image pool consists of 100 (LT1) Landsat 4-5 TM and 193 (LT1) Landsat 7-ETM+ scenes (WRS 2 path8/row47) acquired from the US Geographical Survey (USGS) Global Visualization Viewer for the years of 1984 to 2014. We did not acquire Landsat 8 imagery (starting in 2013) because we did not have access to the latest processing software version of ENVI that would have been needed to do so. We also did not use the LEDAPS products because at the time of analyses these were only available for Landsat 7 imagery. We wanted to be consistent across our image pool, hence the use of ENVI based analyses on the raw images. The images were pre-georeferenced to UTM zone 19 North Projection using the WGS-84 datum.

The analyses proved challenging because more than 60% of the images are fully or partially obscured by clouds which made it difficult to extract the full extent of the lakes and consequently calculate their surface area. Moreover, 85% of the images have data gaps (stripes pattern) due to the failure of the ETM+ scan line corrector (SLC) on Landsat 7 starting in 2003 which adds another degree

of complexity. Figure 3 shows some example scenes with clouds, data gaps and a combination of both while Table 1 presents the specification of the Landsat Images.

Table 1. Study area Landsat Images specification.

Satellite	Sensor	Year	Number of Bands	Resolution (m)	Number of Available Images	Percentage of the Cloud-Free Scene	Data Gaps
Landsat-4	TM	1988–1992	7	30	9	0%	-
Landsat-5	TM	1984–2011	7	30	91	45%	-
Landsat-7	ETM	1999–2014	8	30	193	49%	85%

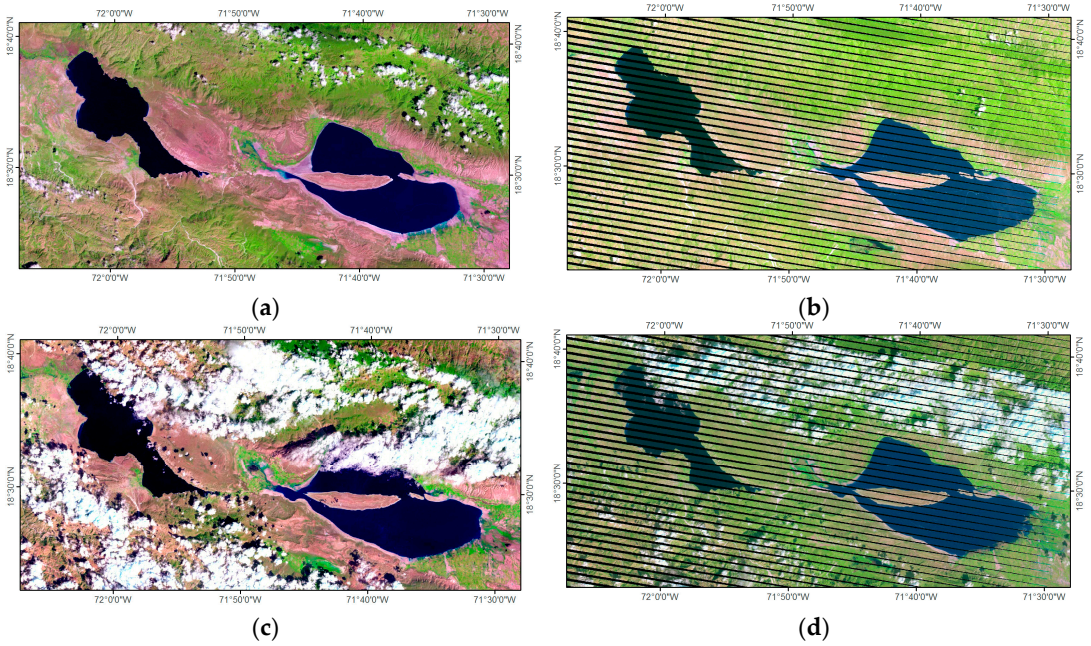

Figure 3. Landsat scene samples contaminated with clouds and data gaps: (**a**) Clear Landsat Image of the lakes (7 October 2002); (**b**) Landsat Image of the lakes with stripes/no data gaps (15 August 2006); (**c**) Landsat Image of the lakes covered with clouds (22 February 2001); (**d**) Landsat Image of the lakes with stripes and covered with clouds (2 December 2005).

Images recorded by satellite suffer from the influence of atmospheric scattering and absorption effects caused by ozone, water vapor, distribution of aerosols, and particles in the air [23]. These effects alter the visibility and characteristics of the images in ways so they differ from each other although they were taken from the same scene though at different date and time. In order to eliminate these incompatibilities and "clean" the images for analyses, an atmospheric correction has to be applied to the images so they are on the same radiometric scale. Atmospheric correction includes transforming the digital value of at-sensor radiance (DN) into the physical value of surface reflectance. Although the USGS website has provided atmospherically corrected images for Landsat ETM-7, we decided to use raw images and calibrate all Landsat ETM-7, TM-5 and TM-4 images using ENVI 4.8 software to ensure consistency for all the images used.

We used the Dark Object Subtraction (DOS) method as improved by [24] which is embedded in ENVI to convert at-sensor radiance (digital numbers (DN) of pixels' radiance in Landsat images) into at-sensor reflectance and from that to surface reflectance using sun position and solar azimuth angle information as well as date and time of the image taken available in the image meta-data. All 292 TM and ETM images acquired for the scene were processed using the same technique and subsequently calibrated for the lakes' shoreline extraction.

2.3. Water Body Extraction

The presence of shallow topographic features dominated by wetlands and agricultural areas poses a challenge when trying to extract lake shorelines, e.g., the shadow of the mountains, wetlands, and also the shadows cast by clouds present "darker" areas that can be mistaken by the analysis algorithm as water surfaces. Thus we needed to introduce some degree of filtering that would eliminate anomalous pixels from the scene/waterbody pixels. For example, "wetland" pixels only cause a problem when trying to detect the lake shoreline on the east and west side of Lake Enriquillo (Shown in Figure 4) and mountain shadow (hill shades) only exists on the south side of Lake Azuei where the lake is surrounded by high mountains that would cast, at a specific time of the day, a shadow toward the lake due to the sun position (shown in Figure 5). Therefore we decided to process the images separately for each lake.

Figure 4. Lake Enriquillo Landsat Image taken on 26 December 1999; red circle shows where wet lands are situated.

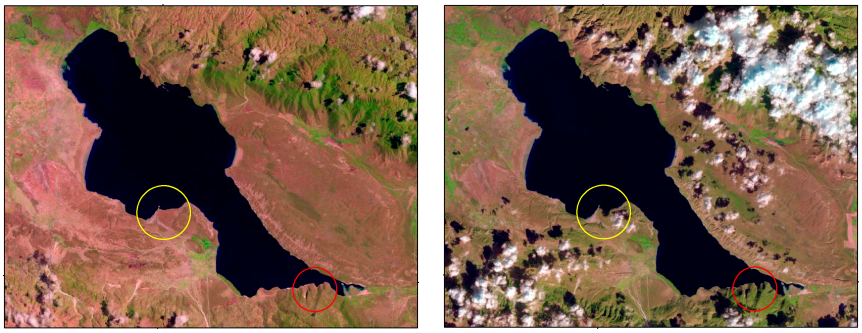

(**a**) (**b**)

Figure 5. Lake Azuei Landsat Image taken on: (**a**) 31 July 1986 and; (**b**) 4 January 1989; red circles on both images shows where hills are situated and how their shades may cause conflict in extracting Lake Azuei outline, yellow circle shows how cloud shadows might distort the lake's outline.

2.4. Cloud and Shadow Detection

One of the problems in using satellite images is the presence of clouds which often obscure the scene, restricting analyses for the dates and the years for which less cloud-free images exist. Unfortunately, only a relatively small percentage of the images are ideal in the sense that they permit a clear and unobscured view of the lake leaving a very limited number of images to work with. Since our goal was to use as many images as possible to get as detailed a time series as we could, we had to find ways around the prevailing lack of "cleanness". One aspect that helps is that since in this study we are only interested in the extent of the lakes we can consider images of feature clouds that have not blocked the lakes' shoreline as a cloud-free scene. Refer to Table 1 which gives a summary of the information regarding what is the percentage of available cloud-free scenes.

Since Clouds are characterized by having a high solar reflectivity at visible wavelengths compared to the reflectance of other surfaces [25], spatial differentiation and thresholding techniques can be applied to distinguish clouds from other features [26]. Various automated detection methods have been developed to detect and mask out clouds and cloud shadows [26–34]. Martinuzzi et al. [25] developed a simple cloud and cloud shadow masking method for tropical landscapes. They applied their method in Puerto Rico and suggested that the method can be used for Puerto Rico's adjacent islands landscape analyses as well. Since the island of Hispaniola has a similar climate to Puerto Rico due its proximity, we decided to apply the same method Martinuzzi et al. had suggested for distinguishing clouds. Band 1 which is an optical band and band 6.1 which represents a thermal band were used in this method. In thermal bands, clouds appear in dark tones (cooler), whereas warmer surfaces have brighter tones, consequently using a thermal band along with the optical band is suitable to detect clouds [25,30,35].

Typically two types of shadows are present in the scene: cloud shadows and topographic shadows (mountain shadows). These shadows are falsely classified as water when using water index methods since they are characterized to be dark and cold [27,35]. Cloud shadows are distinguishable using both geometrical and spectral techniques [28]. These techniques are based on combining spectral methods with finding the geographic position of shadows based on the location and height of clouds and the sun illumination angle [25,28,29,31,32]. Using spectral techniques, on the other hand, shadows can be detected using Near Infrared band (NIR-TM Band 4), and Short Wave Infrared band (SWIR- TM Band 5) [31,35]. In fact, using spectral methods is simpler and less time consuming than alternative approaches and the results they produce have the accuracy of what we need in this study, thus we decided to use these methods for masking out cloud shadows.

Mountain shadows, on the other hand, can be detected by their geographic position using topographic maps [25,28]. A Digital Elevation Map (DEM) for Hispaniola is available in 30 m resolution and can be downloaded from USGS' Earth Explorer website. We used the DEM (data collected in 2000, published in 2008) to find the location of those specific hills and detect the pixels associated with those places from the images. Knowing the current lake level, we set up a threshold for elevation so if the elevation of any pixel identified falsely as water body is bigger than the threshold, its value is going to be substituted automatically to a synthetic value other than water body pixel value. Identifying clouds, cloud shadows, and topographic shadows allow us to approximately find contaminated regions and mask them out of the scene by giving them a value other than water and land surface.

2.4.1. Water Indices

Between general feature classification methods and spectral water index methods, the latter has been identified to produce better results for extracting water bodies [36]. Spectral water index methods are based on the difference of the spectral change trend of all the ground objects through a visible band, usually green, and an Infrared band [37]. The spectral reflectance of lake water is usually lowest in NIR (TM Band 4) and SWIR (TM Bands 5 and 7) bands in comparison with the other land surfaces such as vegetation, build-up lands etc. [38,39]. Using this spectrum property, multi-band methods or spectral water index methods are designed to increase the distance between waterbodies and other ground surfaces [37]. The widely used indices for water body extractions are Normalized Difference Water Index (NDWI) [40], Modified Normalized Difference Water Index (MNDWI) [38], Normalized Difference Moisture Index (NDMI) [41], Water Ratio Index (WRI) [42], Normalized Difference Vegetation Index (NDVI) [43], and Automated Water Extraction Index (AWEI) [44].

The NDWI proposed by McFeeters (1996) uses the green (TM band 2) and near-infrared (TM band 4) to delineate open water features. In 2006, Xu replaced band 4 with band 5 in the NDWI formula suggesting a new water index called MNDWI in order to modify the inability of NDWI in discriminating built-up surfaces from water pixels [38]. NDMI, WRI, and NDVI indices which are mainly used to detect other features were also suggested to be useful in delineating water in some cases [41–43]. Feyisa et al. [44] introduced two automated water extraction indices of AWEInsh and

AWEIsh for identifying water features in cases where no shadow is present in the scene and when the scene is contaminated with shadow, respectively. Differences between these methods result from their changing ability to accurately identify different water body types; meaning water indices work differently depending on the type of water such as lakes, rivers, deep or shallow water, etc. [45].

A waterbody itself has two types of pixels. One is clean and deep water which has a stable spectral profile and the other type is the pixels associated with shallow water not having stable characteristics. Deep-water pixels (pure) can easily be separated from land while shallow (mixed) pixels are more problematic. Based on topological characteristics of the water body, it may contain both pure pixels in its deep section and mixed ones at the edges [39]. In 2014, Jiang et al. [39] stated that based on the type of land surfaces in the study area, water indices may have different performance when applied to different inland water bodies, because they are sensitive to noise such as mountain shadows, vegetation, and built-up land or urban area. For example, when urban land is present, NDWI is most likely to confuse the land pixels with water pixels, while the AWEInsh struggles in the presence of mountain shadow pixels where the NDWI shows the best performance [39]. Hence, the selection of an adequate water index suitable for a specific study site must also be chosen based on the surrounding landscape characteristics and not just the water body alone.

In order to determine the surface area of the lakes, the water indices for each lake domain needed to be computed separately because preliminary analysis of the lakes showed that their topographical characterizations are different from each other although they are located only three kilometers apart. Lake Enriquillo bathymetry features extremely shallow sections on its western and eastern sections while being deep in the center. Lake Azuei on the other hand mostly has defined steep shores (except a shallow part of the northwest side of the lake) while being deep elsewhere. These topographic differences mean that the two lakes have different image characteristics, making it difficult to analyze both lakes as a single feature/in the same image. Lake Enriquillo's mostly shallow shoreline dictates the use of a different index threshold when compared to the one applied for Lake Azuei. For example, applying only the index threshold used to separate water from wetland for Lake Enriquillo would cause the algorithm to interpret hill shades as waterbody while extracting the shoreline for Lake Azuei. Hence, we analyzed each lake separately applying the NDWI, NDMI, MNDWI, WRI, NDVI, and AWEI indices to find out which index has the best performance when extracting the water body while minimizing the effect (error) of misinterpreted wetland, cloud shadow and hill shades.

In order to test the WIs performance for differentiating land and water along the shore (to get the shoreline right but not to carry out a full classification of the entire scene) in shadowed areas, wet lands and shallow water, we just considered two classes: water and land. In order to avoid erroneous calculations resulting from counting water pixels in the land surface areas, we first removed all land-water pixels before setting out to accumulate all water body pixels for further processing. And, Figures 6 and 7 show the result of applying different water indices on the lakes images.

Tables 2 and 3 show the quantitative evaluation and visual inspection of the water indices.

Table 2. Summary of performance evaluation of the water indices used for differentiating land and water pixels along the Lake Enriquillo's shore. (See 2.4.1 for full abbreviations)

WIs	Surface Area Error (%)	Overall Accuracy (%)	Kappa Coefficient	F-Overlapping (%)	Omission Error (%)	Commission Error (%)	Visual Inspection
NDWI	−0.68	99.997	0.99	99.32	0.68	0.00	Good
MNDWI	+4.20	99.97	0.96	92.68	5.82	1.69	Detects wet land as water
NDMI	+209.94	99.09	0.46	29.78	5.93	69.65	Not good
WRI	+1.38	99.99	0.99	98.28	0.18	1.55	Detects wet land as water
NDVI	−1.01	99.996	0.99	98.99	1.01	0.00	Unable to detect shallow water
$AWEI_{nsh}$	+5.23	99.68	0.93	83.57	4.62	1.43	Detects wet land as water
$AWEI_{sh}$	+1.11	99.99	0.99	98.85	1.18	1.02	Good

Table 3. Summary of performance evaluation of the water indices used for differentiating land and water pixels along the Lake Azuei's shore.

WIs	Surface Area Error (%)	Overall Accuracy (%)	Kappa Coefficient	F-Overlapping (%)	Omission Error (%)	Commission Error (%)	Visual Inspection
NDWI	−0.87	99.72	0.99	98.79	1.04	0.32	Good
MNDWI	−4.48	98.85	0.97	95.09	4.70	1.42	Unable to detect hill-shade on the shoreline
NDMI	+32.29	90.17	0.75	69.41	11.36	28.06	Not good
WRI	−1.59	99.63	0.99	98.41	1.59	0.48	Good
NDVI	−29.69	93.04	0.78	70.31	29.69	8.33	Not good
$AWEI_{nsh}$	+2.41	99.37	0.97	87.64	3.22	1.36	Unable to detect hill-shade on the shoreline
$AWEI_{sh}$	−1.81	99.51	0.98	98.03	1.79	0.68	Good

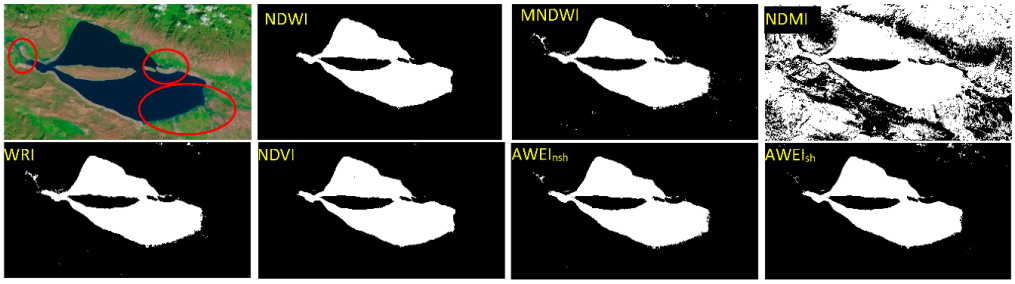

Figure 6. Visual Inspection of the performance of the water indices for Lake Enriquillo.

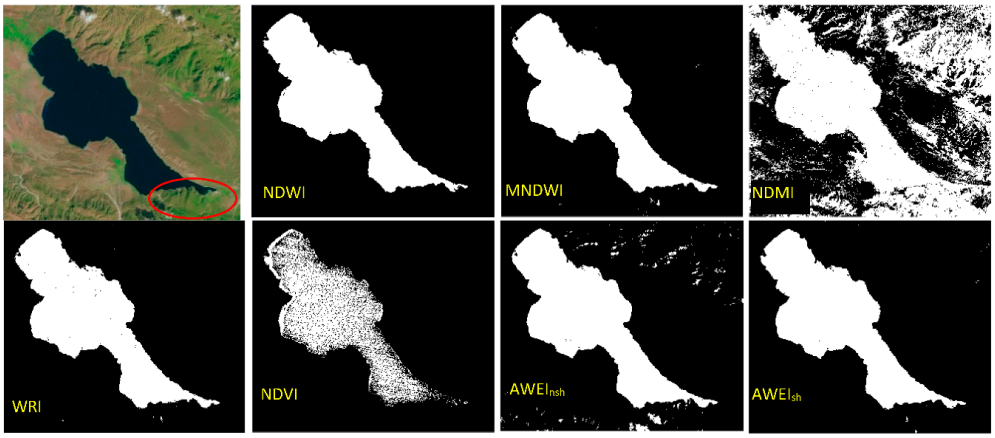

Figure 7. Visual Inspection of the performance of the water indices for Lake Azuei.

Since the surface area of the water body changes throughout time, sometimes growing and creating shallow water areas to expand and at other times shrinking and leaving wetland behind, we needed a water index that can differentiate these features and their associated pixels. We used quantification of (total) surface area error, overall accuracy, Kappa Coefficient, F overlapping, and Omission and Commission error, along with visual assessment in the selection of the best index. It turned out that the overall accuracy of all indices were relatively high, so we used the surface area error and omission and commission error to differentiate between their performances. The results show that except the NDMI, all indices have relatively high performance levels in detecting water pixels. NDWI, NDVI WRI, and AWEIsh showed acceptable results for Lake Enriquillo while for Lake Azuei, NDWI, WRI, and AWEIsh worked better. We chose to use the NDWI, because it had better performance in differentiating mixed water pixels for both lakes, and also featured the smallest surface area error.

2.4.2. Gap Filling

A processed image includes pixels with different values for land, water, clouds, cloud shadows, and hill shades. In order to make use of most images as far as lake outline blockage allows, we needed to detect whether any pixel of cloud, shadows, and hill shades situated next to water body belongs to the lake or not. Toward this end, we decided to treat these pixels as "no data" value pixels while filling their values using a suitable gap-filling method. There are various techniques suggested for gap filling, such as Compositing [25], Regression [33], Data fusion [34], and Neighborhood pixel interpolation [46,47]. While some of these methods utilize a reference image that uses spectral information all are based on computing a value for "no data" pixels depending on pixels from neighboring pixels. In methods using reference images, contaminated pixels will be replaced with good quality pixels from the reference image. The reference image is usually a preceding or subsequent image to the one in question with as minimal a time gap as possible. This technique seems to work well in cases where the environmental and land-cover changes are not significant over time, so images can be spaced in the temporal domain.

In our case, using neighboring pixels did not give us sufficiently correct information on the decision either to keep a water pixel or to ignore a land pixel in the shoreline area. Hence, we decided to use an approach that introduces a reference polygon that is based on the lakes' outline shapefiles. Working with shapefiles gave us the ability to find the best match for the target shapefile in a straightforward fashion thus avoiding pixel replacement in favor of replacing missing line segments. This approach involved converting all processed images into shapefiles and removing all features with the values other than water body values. Using this method, we were left with only the lakes' shapefile; either those generated from cloud-free and gap-free images or blocked scene images. While the lakes' shoreline created out of clear images/scenes were complete, other shorelines were distorted and were made of discontinued lines having missing parts in between.

We created two groups of lake-shoreline features: ones that are complete and those that are incomplete. In order to turn incomplete into complete features, the incomplete feature outline was compared to all others of the complete group. Using the least mean square method, we selected the one with the best fit and inserted the missing parts of the target feature eventually creating a closed polygon for the lake shoreline. Note that after 2003, all extracted features have had discontinuities due to the failure of the ETM+ scan line corrector (SLC), which coincides with the start of both lakes continuously expanding up to now. This resulted, after the 2006–2007 period, into creating shoreline features at locations hitherto not covered thus dramatically reducing the pool of "complete" features that could be used to substitute for "incomplete" features. In order to compensate for this situation, we started to include more than just one "best" fit feature.

2.4.3. Final Algorithm

Based on the characteristics of the study site and the type of water bodies and noise in the scene, we developed an algorithm to identify and classify noise pixels and remove them from the scene and then detect water bodies using the appropriate water index. In the algorithm, shown in Figure 8, cloud pixels were identified in the scene first because of their distinct spectral characteristics as compared to the other noise types. Band 1 (Blue, 0.45–0.52 mm) and Band 6 (Thermal, 10.4–12.5 mm) fraction worked best for us in extracting clouds. A threshold setting of 0.2 worked effectively and pixels that fell below this threshold were labeled as a cloud. However, out of 192 images total for each lake, 55 for Lake Enriquillo and 59 for Lake Azuei could not be processed due to the high percentage of cloud cover obscuring the scene.

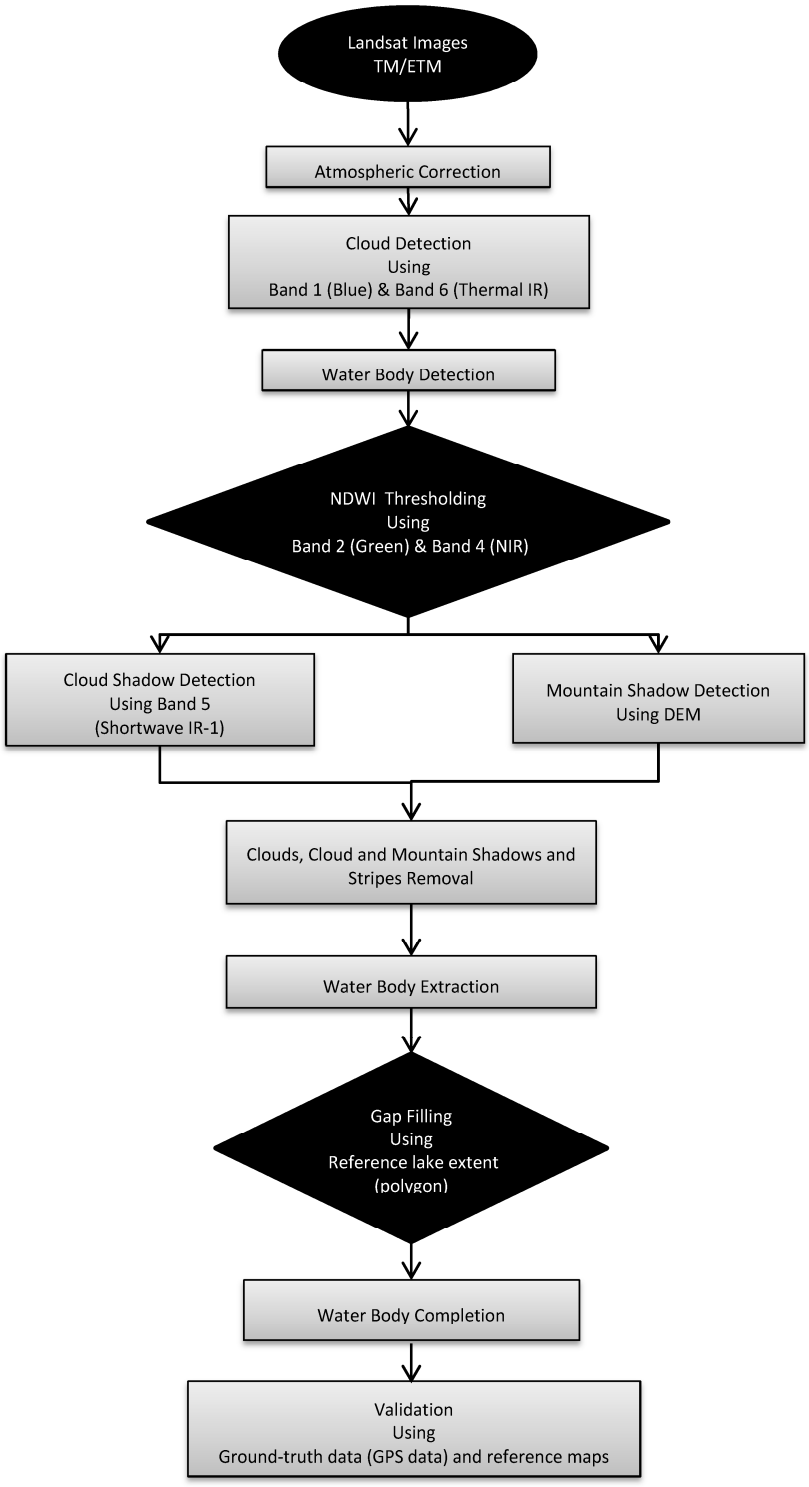

Figure 8. Water Body Extraction Algorithm.

The Normalized Difference Water Index (NDWI) is expressed as:

$$NDWI = \frac{(\rho_{Green} - \rho_{NIR})}{(\rho_{Green} + \rho_{NIR})} \quad (1)$$

where, ρ_{Green} and ρ_{NIR} are the surface reflectance values of Band 2 (green, 0.53–0.61 mm) and Band 4 (Near-Infrared, NIR, 0.76–0.90 mm) in the Landsat TM/ETM. The threshold of zero was proposed

by McFeeters (1996) for extracting water bodies, having positive NDWI values for water pixels and negative values for non-water pixels. Thus, a starting threshold of zero was initially considered for both lakes which were then followed by a gradual adjustment of the threshold to find an optimum value for each lake. For Lake Azuei, the optimal NDWI threshold turned out to be −0.12 while a zero value for the NDWI threshold worked best for Lake Enriquillo. Since both TM and ETM satellite sensors have the same bandwidth, the NDWI threshold for both is the same. Using the same approach we were also able to address the wetland issue.

After identifying water body pixels all resulting water pixels were examined to see if they were mixed in with shadows. Using the Digital Elevation map and also the Short Wave Infrared band, both topographic and cloud shadows were detected from the group of mixed water pixels. We also considered a buffer of one-pixel size around cloud and their associated shadows to make sure that they are completely removed from the scene. Figure 9 shows one of the Landsat images before and after the process and also the classified image of detecting different pixels. After identifying all non-water pixels they were removed from the scene along with the land surface pixels. This step was followed by the creation of the lake's feature shoreline where the missing or incomplete parts were completed using one or more reference images, as described earlier.

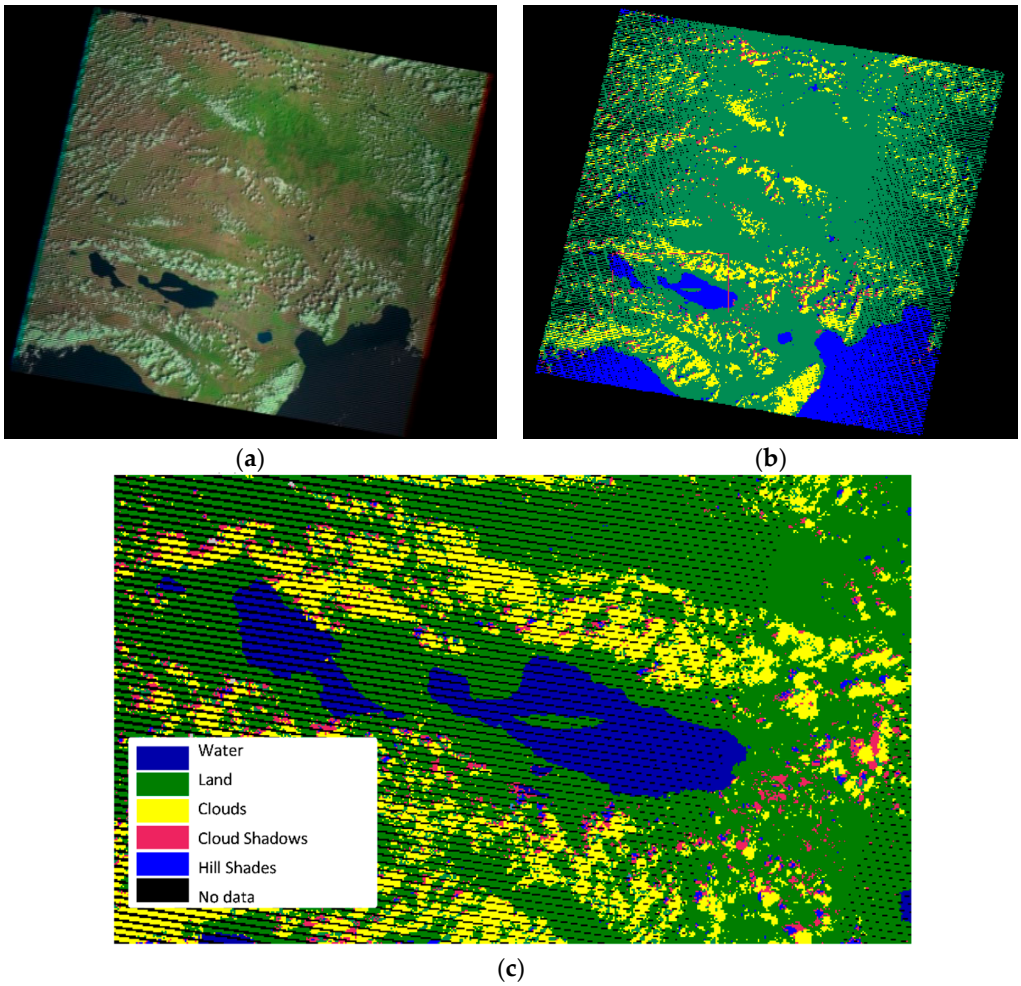

Figure 9. (**a**) Landsat Image taken on 21 February 2012 (path8/row47); (**b**) Processed Landsat Image; (**c**) Study Area Classified Image.

When all non-water pixels were identified, they were removed from the scene along with land surface pixels. Then lake feature/lake's feature outlines were created and their missing parts were

completed using one or more reference images. Figure 10 shows an example of a lake's feature which has been extracted from the image taken on 21 February 2012 and completed using a reference image. The target lake outline is derived using the February Landsat image which was completed using a reference outline from 20 January 2012. Figure 10a,b shows the target Landsat image and the extracted outline, respectively and Figure 10c,d shows the reference image and the lake's outline. For this sample only one reference image was used, although in some cases more than one reference image was needed.

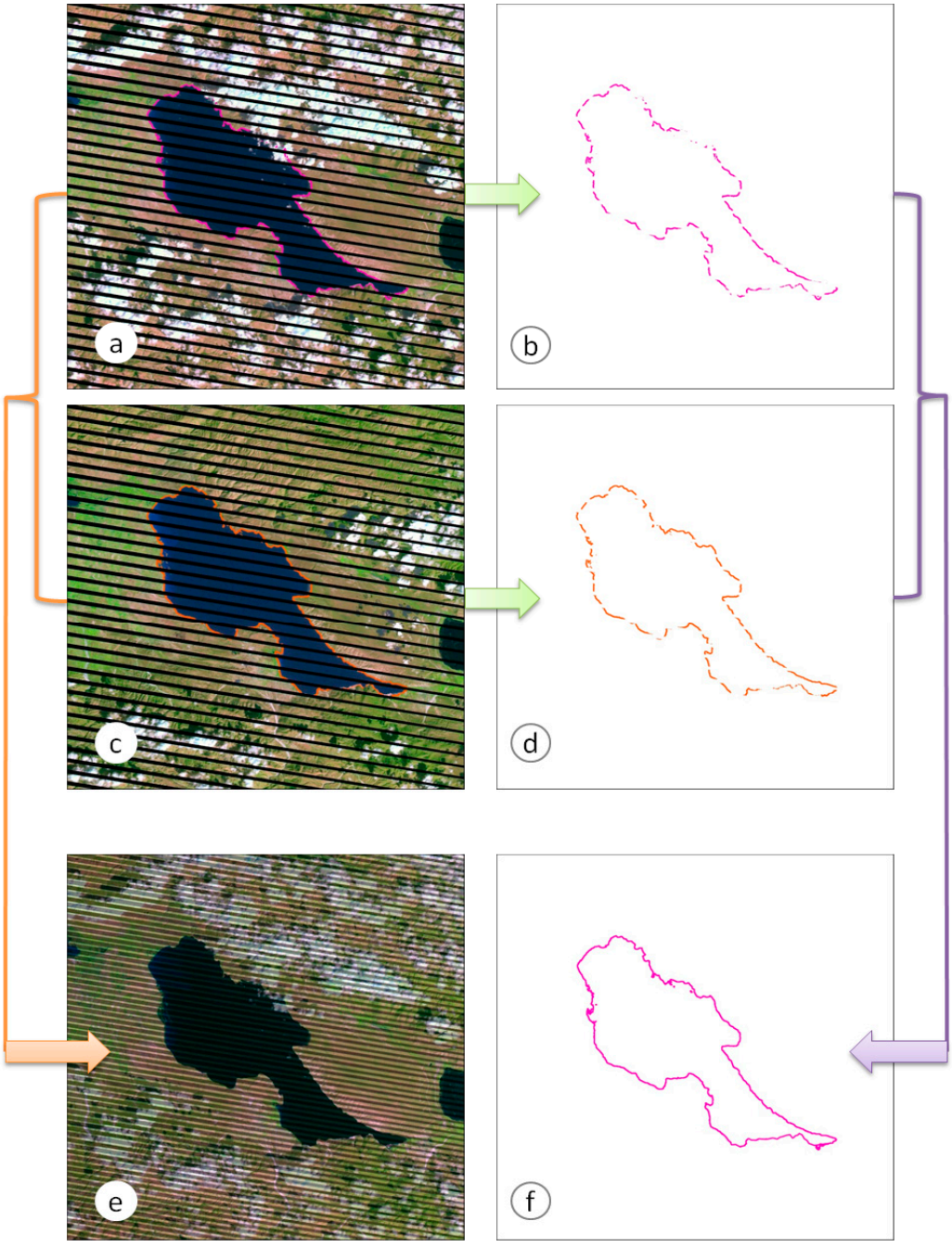

Figure 10. Completed Lake Azuei polygon: (**a**) Landsat image taken on 21 February 2012; (**b**) Lake's outline created using image on 21 February 2012; (**c**) Landsat image taken on 20 January 2012; (**d**) Lake's outline created using image on 20 January 2012; (**e**) Image created from overlaying two Landsat images of (**a**,**c**); (**f**) Lake's outline created using (**b**,**d**) outlines.

2.5. Validation of Image Analyses

During two field campaigns in 2013, we collected bathymetric data for the two lakes. The generated tracks, referenced with Lat/Lon, included many alongshore sections (before turning back to another leg of a general zig-zag pattern crossing the lakes) that we decided to use as a second set of data to compare to the lake shoreline polygon (in these sections) as extracted from the satellite images. To assess the general validity of the results we first selected those track segments that mapped the shoreline and then measured the distance between the track of the boat and the lakes' extent. Near steep edges the boat could get to within a few meters of the shore while in shallower areas the boat needed to stay back, up to several hundred meters in very shallow areas (Figure 11a). Nevertheless, since all GPS data was taken from inside the water body it should also be inside the extracted lake extent. While this was true for the vast majority of points we observed that some fell outside (Figure 11b). In order to have a better understanding of the extent of these "misses" we computed minimum distance, maximum distance, mean distance, and standard deviation for each lake as summarized in Table 4. The results showed that for Lake Enriquillo, the distances (track location minus polygon location) are between 0.17 (minimum) and 17.05 (maximum) meters with an average of 3.67 m and a standard deviation of 2.42 (Figure 12a). For Lake Azuei the minimum and maximum distances are 0.03 m and 36.58 m, respectively with an average of 8.38 m and a standard deviation of 6.33 (Figure 12b). Considering the fact that the resolution of the Landsat images is 30 m/pixel, these errors fall well within or at least close to the image resolution thus demonstrating a good degree of accuracy on image analysis.

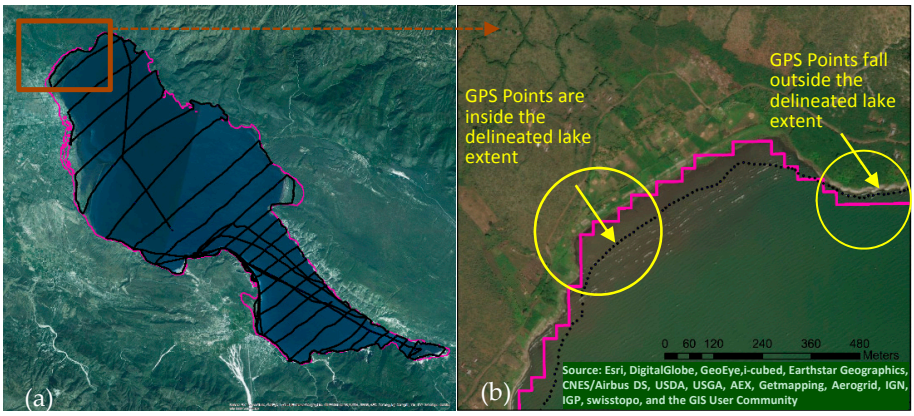

Figure 11. (**a**) Black line is the boat track of GPS points and the pink line is classification result for the Landsat image taken in 1 July 2013; (**b**) Position of GPS data in comparison with the extracted lake extent.

Table 4. Comparison of classification results with GPS data.

Date of Gathering GPS Data	Landsat Image Date	Image Quality	Lake	GPS Points Position	Maximum Distance (m)	Minimum Distance (m)	Mean Distance (m)	Standard Deviation
25–26 March 2013	27 March 2013	-Clear scene -Existence of gaps	Enriquillo	GPS points fall inside the delineated lake extent	94.57	0.18	41.07	32.75
				GPS points are outside the delineated lake extent	17.05	0.17	3.67	2.42
19–24 June 2013	1 July 2013	Existence of: -Gaps -Cloud -Cloud shadow	Azuei	GPS points fall inside the delineated lake extent	89.61	0.03	35.25	21.51
				GPS points are outside the delineated lake extent	36.58	0.03	8.38	6.33

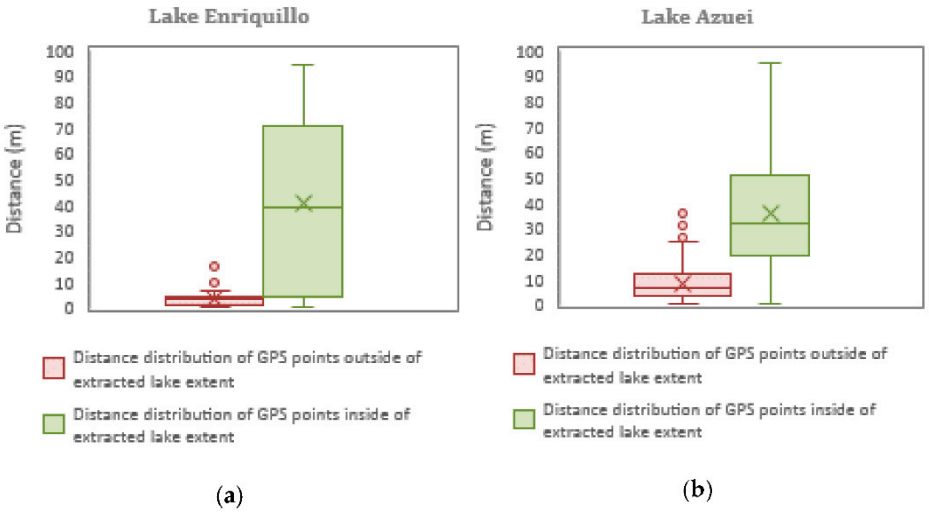

Figure 12. (**a**,**b**) Distribution of the values of the distance between GPS points and the lake extent.

As an additional step we chose three images for each lake from our pool having a mix of clear and problematic scenes and then overlaid these with referenced lake polygons that we manually generated using GIS tools. Table 5 shows the accuracy assessment of the results in comparison with the reference maps.

Table 5. Summary of classification accuracy using reference maps.

Lake	Date	Conditional Kappa for Water Body	F-Overlapping (%)	Overall Accuracy (%)	Surface Area (km^2)	Absolute Error (km^2)	Relative Error (%)
Enriquillo	22 February 2001	0.989	98.72	99.76%	206.036	0.53	0.26
	19 September 2007	0.992	98.31	99.64%	231.977	0.71	0.31
	21 August 2014	0.992	98.97	99.68%	346.694	0.30	0.09
Azuei	22 February 2001	0.995	98.59	99.67%	118.368	0.56	0.47
	19 September 2007	0.993	98.46	99.63%	119.296	0.20	0.17
	21 August 2014	0.980	98.08	99.47%	137.277	1.08	0.79

Three images from the years of 2001, 2007, and 2014 were selected and the accuracy statistics consisting of conditional Kappa (only for water body), F-overlapping, and overall accuracy were calculated for each lake using a scripted tool [48]. We also computed the absolute error (the surface area difference between the produced water body and the reference map), and the relative error (absolute error over the surface area of water body in the reference map) to see how much error would be introduced to the surface area values by our classification method. The overall accuracy for both lakes yields a value of more than 99% agreement, a conditional kappa coefficient of more than 98%, and an F-overlapping percentage of more than 98%. Relative errors are also small and less than 1%, which demonstrates a high degree of accuracy in surface area estimation even though there are miss classifications of a few hundred pixels in each case; these do not significantly affect the accuracy however.

3. Results

3.1. Lake Time Series

3.1.1. Previous Work

Although the extent of Lake Enriquillo's surface area has been published in several reports over the years there have been few attempts to examine surface area change dynamics of the

lake [9,11–14,18,19,49–52]. The Instituto Nacional de Recursos Hidráulicos (INDRHI) and the Water Center for the Humid Tropics of Latin America and the Caribbean (in Spanish- Centro del Agua del Trópico Húmedo para America Latina y el Caribe (CATHALAC)) are perhaps the best-known data sources for Lake Enriquillo. In 2009, CATHALAC published seven values for the lake surface area from 2000 to 2009 two of which were calculated based on the Landsat Images while the remaining five were based on MODIS data [9,12,18,50,51]. In 2012, CATHALAC published a new set of lake surface area data spanning the years from 2007 to 2012, which turned out to be different from the ones presented in 2009 [51]. Logan et al. [12] showed two time series of surface area, one of which is taken from the CATHALAC-2009 paper, while the other one was referenced to INDRHI data generated from Landsat images. There are two other groups, i.e., Programa de Naciones Unidas para el Desarrollo (PNUD) and Universidad Autónoma de Santo Domingo (UASD), that produced some surface area information for the lake as well [52]. The UASD values seem to have been averaged over the reported years of 2004, 2011, 2012, and 2013 even though it remains unclear if these values have been computed from averaging several images over a specific month or just using any image as a representative for a specific month.

Another source of data is the Coastal Urban Environmental Research Group (CUERG) at the City College of New York which publishes lake data on their Webpage called "The Hispaniola Lakes Project" [53]. They used Landsat imagery to calculate the surface area of both Lakes Azuei and Enriquillo starting from 1979 until 2015 using about 50 data points for Lake Enriquillo. Schubert [19], Méndez-tejeda et al. [11], and Luna and Poteau [14] present average surface area values for Lake Enriquillo also having used Landsat Imagery. The newest time series available for both Lakes is the one produced by Wright et al. in 2015 [13]. They too used Landsat Imagery to calculate surface area for both lakes even though they do not reference all data they used. We have summarized all sources of lake surface area in Table 6 (for Enriquillo) and Table 7 (for Azuei).

Table 6. Lake Enriquillo surface area time series references.

Source	Timespan	Number of Data Points	Range of Values km^2	Data Used
INDRHI [12,17]	2000–2012	14 *	160–320 km^2 *	Landsat Imagery
CATHALAC, 2009 [9,18,50,51]	2000–2009	7	205–312 km^2	Landsat/MODIS
CATHALAC, 2012 [51]	2007–2012	9	234–340 km^2	-
PNUD [52]	2000–2013	7	205–369 km^2	-
UASD [52]	2004–2013	4	231–404 km^2	-
CCNY [53]	1979–2015	50	165–353 km^2	Landsat Imagery
Schubert, 2003 [19]	1969–2002	7	165–269 km^2 *	-
Luna and Poteau, 2011 [14]	1982–2010	24	195–332 km^2	Landsat Imagery
Wright et al., 2015 [13]	1984–2013	60 *	231–325 km^2 *	Landsat Imagery
Mendez et al., 2016 [11]	1996–2013	9	22–46 km^2	-

* The data is retrieved from the graph presented by the reference and the values are approximate.

Table 7. Lake Azuei surface area time series references.

Source	Timespan	Number of Data Points	Range of Values km^2	Data Used
CATHALAC, 2012 [54]	2007–2012	9	119–137 km^2	-
CCNY [53]	1979–2015	47	111–140 km^2	Landsat Imagery
Luna and Poteau, 2011 [14,49]	1985–2011	21	113–132 km^2	Landsat Imagery
Wright et al., 2015 [13]	1984–2013	49 *	121–133 km^2 *	Landsat Imagery

* The data is retrieved from the graph presented by the reference and the values are approximate.

3.1.2. Time Series Development

The "Lake Extent"-time series was produced after passing all images through the analyzing tool we described earlier spanning the period starting in 1984 to 2014, i.e., about 20 years of coverage. We noted that the image pool had several gaps the most significant from May 1984 to January 1986 and

from July 1992 to July 1996, i.e., 2 and 4 years respectively as shown in Figures 13 and 14. Examining the general time series patterns of both lakes two significant behaviors stand out: firstly, before 1998 the lakes show an uncorrelated growth and recede pattern, i.e., they expand and shrink at a random synchronous or asynchronous rate suggesting that the two lakes exhibit dynamics that are mostly independent, even though one cannot fully rule out some impact due to lake level differences. Secondly, the two lakes align their general behavior after 1998 with a first strong growth-recede pattern from 1998 to 2004 after which the dramatic growth period starts peaking in 2014 with a 2.3 (Enriquillo) and 1.2 (Lake Azuei) increase in surface extent when compared to 2004. Note that the surface area extent dynamics alone do not indicate proportional or non-proportional growth/shrink correlations between the lakes because of the lack of bathymetry and surrounding DEM inclusion. While surface area extent is our primary data entry point a much more meaningful comparison is the total volume increase, relative volume increase, and the ratio of volume increase to associated drainage area to discern values and indices that allow for comparison. While the general growth trend from 2004 to 2014 is the most significant in view of the societal impact because of the many inundations and subsequent loss to land and property, shorter term (seasons or even monthly) patterns that are superimposed on the 10-year growth remain as uncorrelated and appear to follow lake specific dynamics.

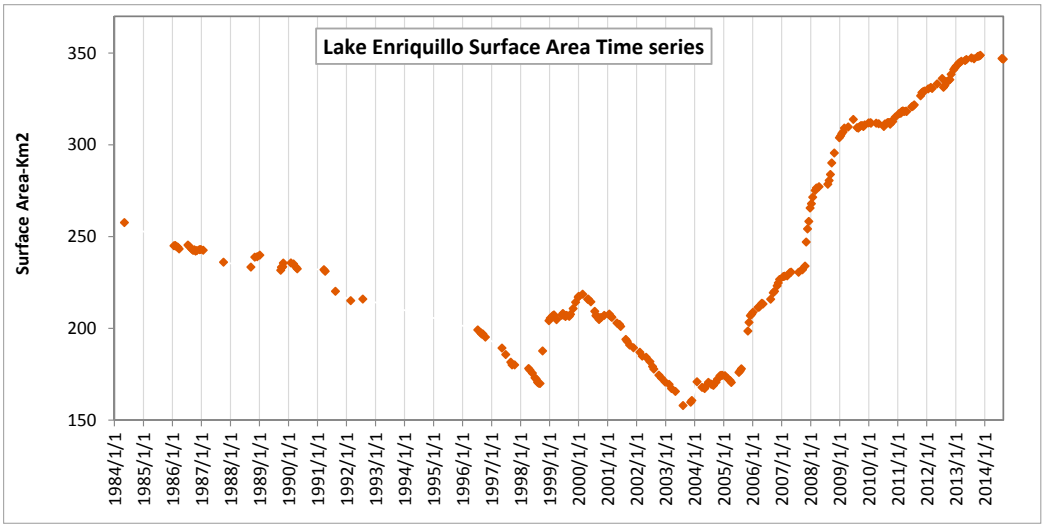

Figure 13. Lake Enriquillo surface area time series.

Figure 15 shows the surface area data series for Lake Enriquillo. Straight lines in the graph mean a gap in data series whether there is or there is not any satellite image available for corresponding dates. Note the data gaps between the years of 1993 to 1996 which is, as mentioned before, due to the lack of Landsat images for those years. Imagery production resumed in June 1996 and it took until 2004 for the production to be no less than 12 a year, i.e., recording frequency increased. It should be noted that we eliminated the Méndez-tejeda et al. data series [11] because it did not present the same range and also was off by a factor of almost 10. It is clear from Figure 13 that all references capture the general trends represented by the steady shrinkage from 1982–1998, the 1998–2004 spike and then the "grand growth, GG" from 1996–2014. Straight lines, such as in the in Luna and Poteau series [14] (for 2003 to 2006) and 1999 in Wright et al. series [13] are due to lack of data compiled for these years. Other deviations, such as over and undershoots, which vary in extent between the data sets and are not consistent within or across data sets can also be due to variations in Landsat image analyses, i.e., cloud cover and shadow removal which can lead to local oscillations from one image to the next. The largest difference between the sets arrives from the absolute values between them, namely Luna and Poteau [14], Wright et al. [13], and CCNY which show a generally higher location on the plot than the other references. Although Luna and Poteau [14] and CCNY started almost at the same point with

Wright in 1984, they diverged as time progressed and join the graphs of the other references in 1998. There is much less difference between values observed in our study and others time series, namely Schubert (2003) [19], INDRHI (2012), and CATHALAC (2012). PNUD introduce much higher values for the lake surface area, starting from the period of 2008–2012 and only match the rest of the curve group for 2014. We attribute these differences to the use of different data sources/products such as Landsat, MODIS, and ASTER, in addition to the aforementioned differences in analyses tools.

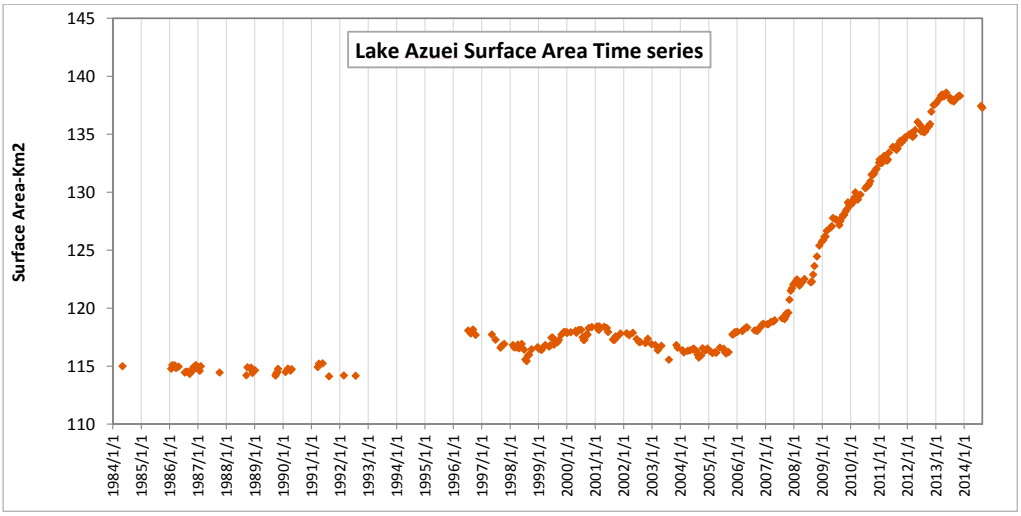

Figure 14. Lake Azuei surface area time series.

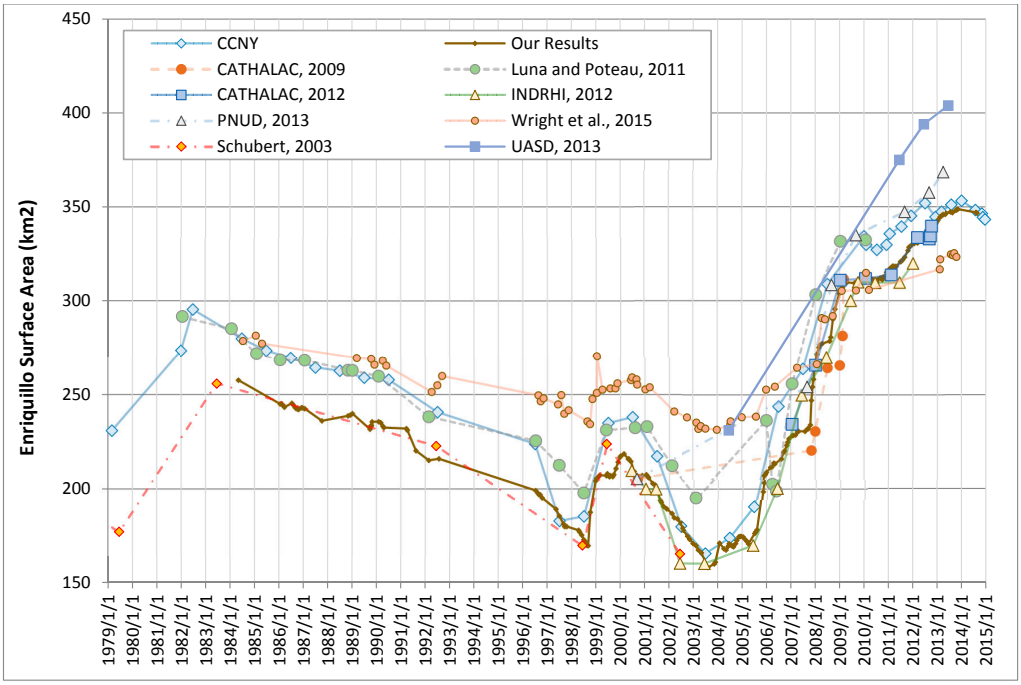

Figure 15. Lake Enriquillo surface area time series comparison.

Figure 16 shows all time-series data we have been able to compile for Lake Azuei in addition to our own data, collected in 2014. Like as for Lake Enriquillo, the data groups agree on the general trends, i.e., a period (1984–2006) with moderate oscillations around a steady mean of 115 km^2 (1984–1996) and approximately 116 km^2 and (1996–2006), then the steady growth (2006–2014). Note though the

Enriquillo spike from 1998–2004 is much less pronounced in Lake Azuei and also that the corresponding GG for lake Azuei starts about two years after that of lake Enriquillo. While the graphs exhibit similar oscillatory behavior as compared to Enriquillo, the most notable feature is that the graph from Wright et al. sits considerably higher than the other graphs for the period of 1984 to 2006 suggesting a substantial difference in how the data appears to have been analyzed. Personal communication (October 2016) with the authors suggest that the discrepancy may be due to the use of yet another data source, i.e., a topographic map of the region created a few years back by another research group which introduced different elevation values for varying lake extent polygons. Like Lake Enriquillo, Lake Azuei features larger time scale processes that are superimposed by smaller time scale ones, the latter of which generate an oscillatory pattern of small amplitude growth and shrinkage. In general, however, the graphs coincide fairly well, much better than the ones (same references) for Lake Enriquillo.

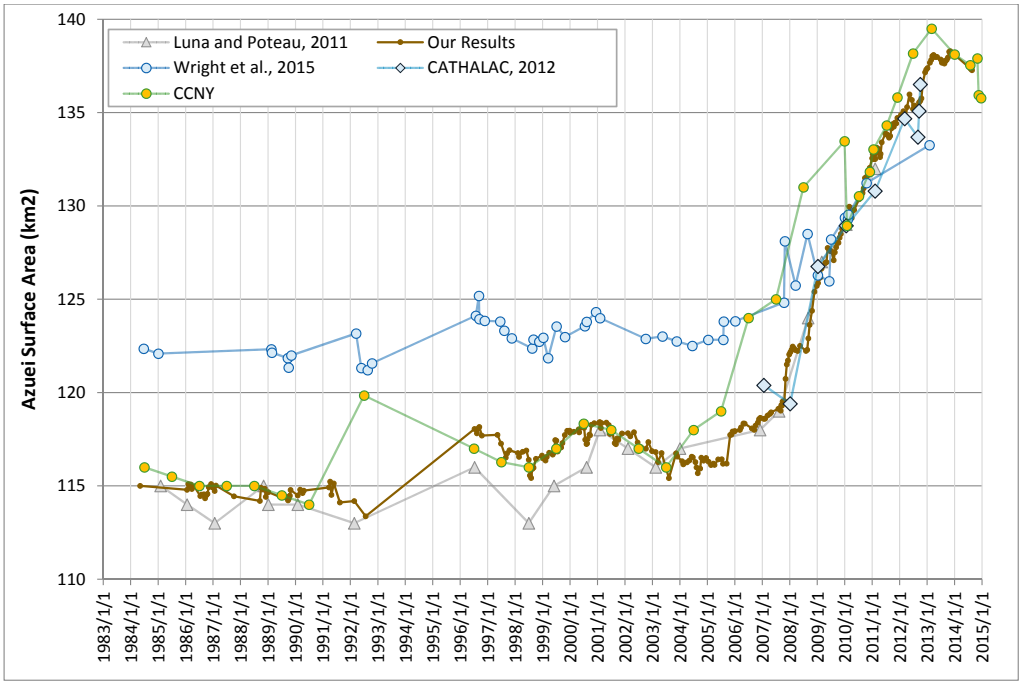

Figure 16. Lake Azuei surface area time series comparison.

3.2. Bathymetric Data

There are five bathymetry maps available for Lake Enriquillo. The first map was created by INDRHI in 1992 [17,49], shown in Figure 17a, featuring contour lines with corresponding elevation data. In 2003, Schubert [19] presented a newer version of the bathymetry based on data collected and prepared by INDRHI (Figure 17c). These two maps both show about the same contour line patterns and also elevation data, even though they differ somewhat in the northern sector of the lake. Unfortunately, neither map product is referenced to a vertical datum and also does not report the dates at which the data was collected (thus denying an opportunity to link it to a Landsat image taken around the same date). Buck and Brenner in 2005, showed a map which was modified from an Araguás-Araguás et al. study done in 1993 (Figure 17b) [10,55]. The map is necessarily similar to the one presented by Araguás-Araguás et al. in 1995, though now featuring lake depth contours instead of elevation. The depths range between 0 to more than 22 m. These bathymetry maps show that the lake is composed of two large bodies of water, separated by Cabritos island. The northern part of the lake is smaller but much deeper in comparison to the southern part. There are also two small hills on the west side of the lake called Islita and Barbarita islands. These two islands can fall dry for low lake levels and disappear below the water surface for higher lake levels.

In 2015, Piasecki et al. [20] and Wright et al. [13] both independently developed a new bathymetry map slightly different from the others' results, showing two small holes on the north side of the lake (Figure 17d,f). Wright et al. [13] used seismic data taken from the study area in 2013 along with Landsat images and past bathymetric maps to build a new contour map with depth values (Figure 17d). The contour lines depict depth between 0 to 24 m, while the stretched color map of the lake beneath ranges between 0 to 32 m. On combining the contour lines with the stretched color map yields two deep depressions each almost 8 m deeper than the 24 m contour line. This presents a sudden change of the bed of the lake, which is difficult to discern on the bathymetry images.

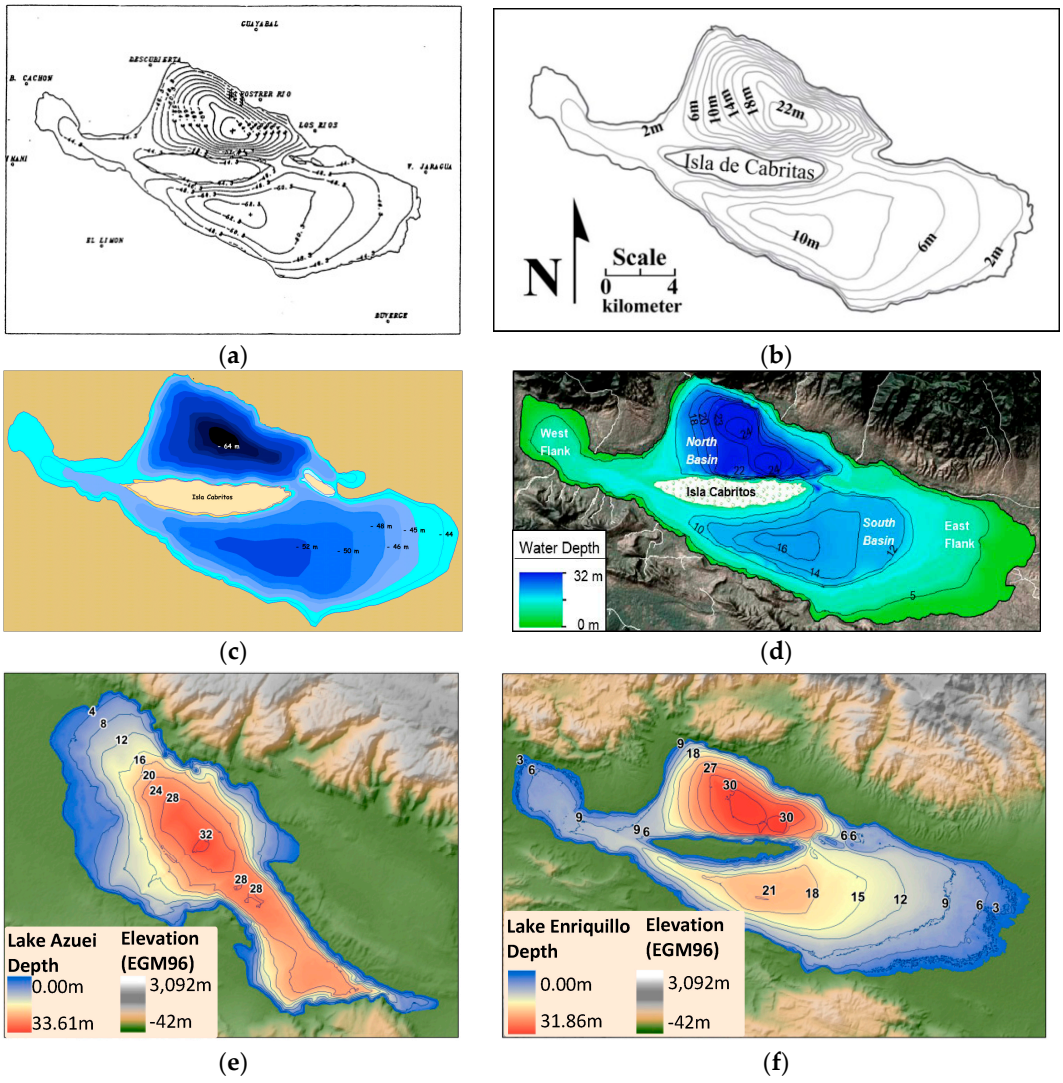

Figure 17. Comparing bathymetry maps: (**a**) Bathymetry map presented by Araguás Araguás et al., 1995 [17]; (**b**) Buck and Brenner, 2005 [10]; (**c**) Schubert, 2003, 2012 [19,49]; (**d**) Wright et al., 2015 [13]; (**e**,**f**) Piasecki et al., 2015 [20].

In 2013, Piasecki et al. [20] carried out several data collection campaigns aimed at obtaining bathymetric data for both lakes, in addition to digital terrain information to create a seamless lake/surrounding terrain model that can be filled and drained to obtain maximum depth, elevation, and volume information. During several trips, sonar data was collected following a zig-zag pattern through both Lakes Azuei and Enriquillo. The data was later analyzed and a bathymetry map was produced using almost 35,000 sonar depth values collected [20,56]. Figure 17e,f shows the bathymetry maps of both lakes.

Maps produced prior to the ones published in the 2013 timeframe [10,13,17,19,49,55] are quite similar. However, they feature significant differences in their shape of contour lines and the presentation of data as elevation or depth makes it difficult to choose between them. Also, most of them do not represent the recent growth (extent) of the lake and it is not stated how the maps were created or what was the date of creation. The one created by Wright et al. [13] seems to feature an unreasonable topography shape which may be the result of using older versions of bathymetric data. Thus we decided to use the map produced by Piasecki et al. [20] as it shows the latest shape of the lake due to the most recent collection campaign. It has also been prepared only using field measured values and is such independent of older data sets; in addition, they presented the only bathymetry map available for Lake Azuei.

3.3. Connecting DEM and Bathymetric Data

Although having surface area time series of the lake gives the ability to observe the behavior of the lakes over time, it is not sufficient to quantify lake responses in terms of quantities that are relevant to the water budget, i.e., volumes added or subtracted over time. To close this gap it is necessary to develop a representation of the bathymetry and if one were to examine future states of growth, "stitch" this bathymetry to the surrounding digital elevation model to form a "bathtub"-model that can be filled and emptied at will. Short of having lake level sensors that track the lake level as referenced to a vertical datum (such as Mean Sea Level) the only way to calculate volumetric changes is to use the lake extent polygons (as described earlier) and slide them down the "bathtub" walls until they fit snuggly around the wall thus yielding the current lake level (Figure 18).

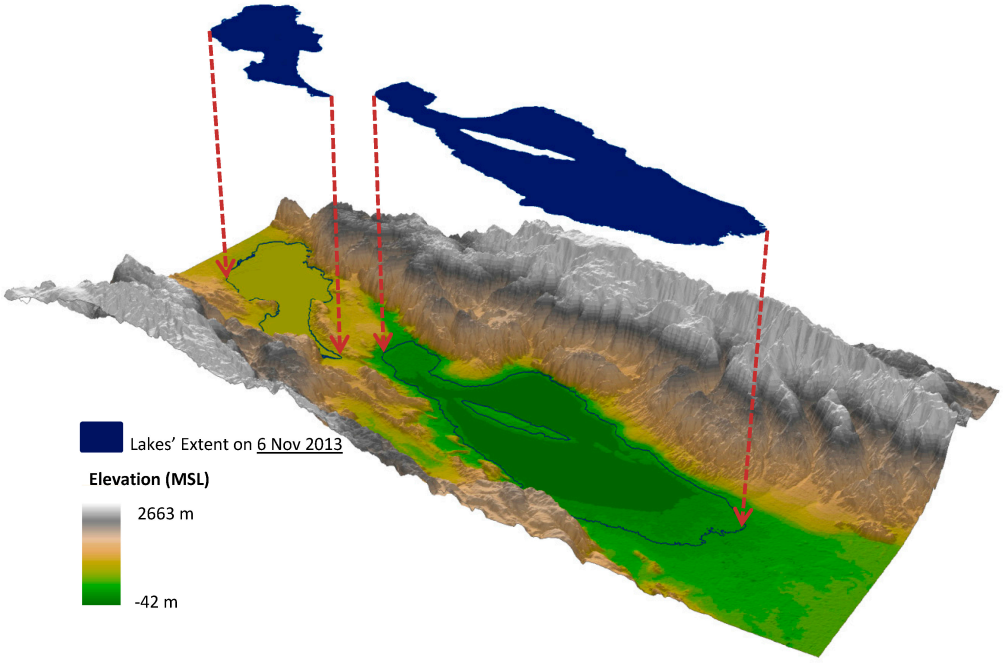

Figure 18. An example of sliding a Landsat Image to Digital Elevation Map (DEM) in order to find the elevation and volume.

Connecting, or "stitching", the bathymetry data set to the surrounding SRTM DEM data set proved challenging because the DEM used the EGM96 (Earth Gravitational Model 1996) datum as a default while the bathymetry data is not referenced at all as the values collected were local, i.e., with respect to wherever the water level was on the day the data was collected. We did not have a geographic control point (GCP) available that would have allowed us to "connect" the lake level to a referenced vertical datum point. In fact, according to the cartography department of the Dominican

Military (personal communication), there is only one GCP available which is about 10 miles to the southeast of the eastern shore of Lake Enriquillo, way too far away for us to be of use.

There are several options on how to overlay the bathymetry on the DEM. The simplest way is to consider one of the lake's extents as a reference line and match it with DEM contour lines and extract the elevation for that specific lake outline. Using that lake outline as a base, all lake elevations in the time series can then be produced using lake surface area and their associated depth. Lastly, all the DEM information beneath that specific contour line is then deleted and the bathymetry map can be connected to the DEM along that lowest contour line. The DEM was published in 2008 and it shows the lake extent/surface at that time with elevation −42 m (EGM96). However, it was unclear when the elevation data was computed for the area with no date given. Because the lake fluctuates even throughout the seasons the lack of a date renders the −42 m elevation almost unusable in our desire to find a proper vertical reference.

When overlaying the bathymetry over the DEM we found that the largest lake extent recorded matches with the contour line of −31.3 m (MSL). Hence, between the two elevations of −42 m and −31.3 m, the DEM and the bathymetry overlap as demonstrated in Figure 19. In the DEM, two contour lines of −31.3 m and −42 m are shown and the corresponding lakes' extents are also marked on the bathymetry. The contour line of −31.3 m corresponds to the lake's shoreline at zero depth (extracted from the Landsat images, taken on 6 November 2013) while the contour line of −42 m corresponds to the lake's shoreline at a depth of 7.6 m (Landsat images taken on 2 October 2006). As can be seen the depth difference between these two contour lines is 10.7 m which is higher than 7.6 m. In other words, matching depth contours of the lake bathymetry to elevation contours of the DEM proves to be inconsistent and thus poses a problem because the resulting lake volumes would also differ.

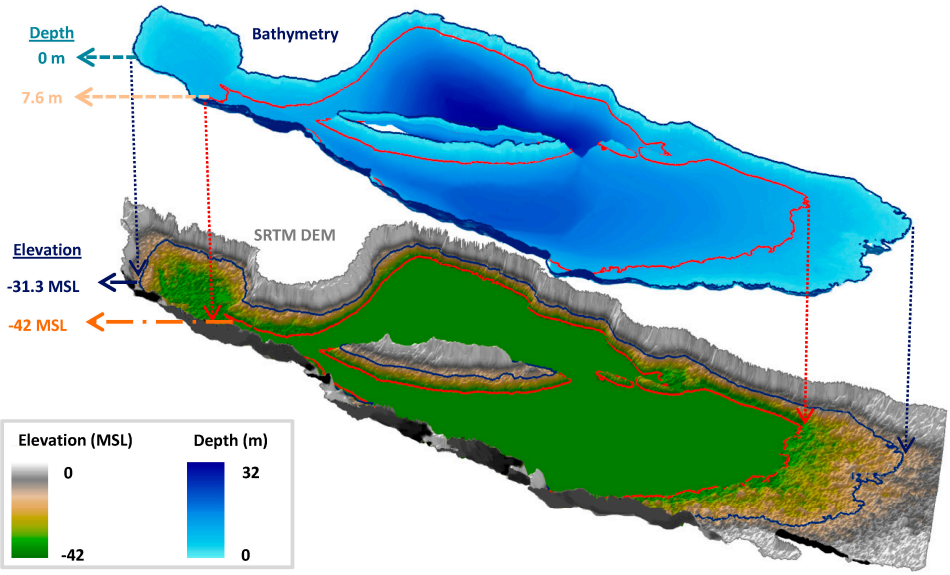

Figure 19. Demonstration of bathymetry and DEM compatibility.

To better demonstrate the problem at hand we use a (hypothetical) cross section as shown in Figure 20. The slope of the DEM between the contour of −42 m and −31.3 m is steeper than that of the bathymetry. Any contour line between −42 m and −31.3 m can be considered as a reference line and the bathymetry model could be placed anywhere between these two contours. We considered the two extremes of −42 m and −31.3 m to see how the connection method affects the lakes' physical parameters. In Figure 20b, the bathymetry is placed using the −31.3 m contour line and all the DEM surfaces below it are deleted. Figure 20c,d shows the condition in which the −42 m contour line is used as the reference. However, these two figures differ in which overlapping surface is preserved. In Figure 20c, the bathymetry is preserved and the DEM is eliminated. This method results in the

formation of a cliff with a height of about 3 m, which is not realistic. On the other hand, in Figure 20d the DEM is kept and the overlapping bathymetry surface is deleted. Both approaches have an effect on the computed volume of the lake (Vb and Vc) which consequently results in a volume other than the real value. Vb is almost 27% of the whole volume of water in Lake Enriquillo and Vc is less than 27% depending on which contour line is considered as a reference line. Even if we were to find a contour line that compensates for the calculated volume and that gives us a real volume in case (d) (Figure 20d), the proper depth allocation remains unresolved. In cases (c) and (d), the bottom of the lake will sit lower; resulting in an increase of depth (shown as D_2 in Figure 20). Hence, in order to reserve volume and depth of the lake, we decided to use the case shown in Figure 20a. This way the bathymetry can be connected to the DEM and for future calculations the error in deriving volume and depth is minimal. The same approach was used for Lake Azuei albeit we decided to take a 6 November 2013 shapefile as the base to extract elevation values and then delete all the DEM parts beneath it substituting bathymetry values instead.

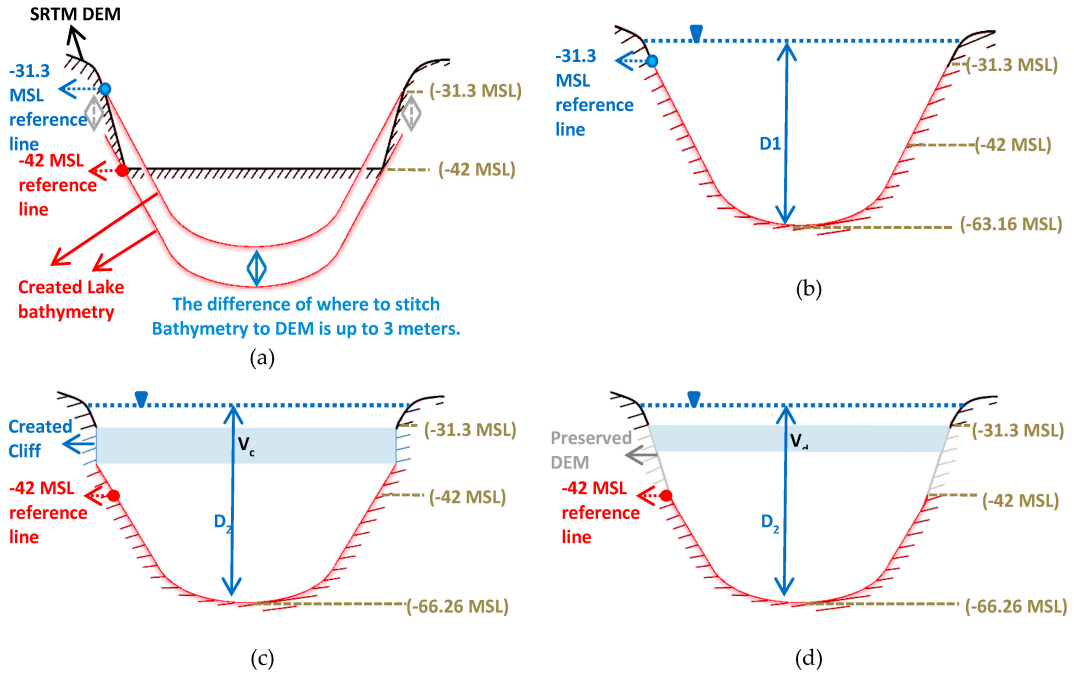

Figure 20. Presentation of different methods for stitching bathymetry to DEM; (**a**) illustration of two possible options for choosing reference line; (**b**) the method using −31.3 MSL reference line; (**c**) the method using −42 MSL, and preserving bathymetry reference line; (**d**) the method using −42 MSL reference line, and preserving DEM.

3.4. Rating Curves

The first application of using the time series and the seamless bathtub model is to create rating curves for Area-Volume and Area-maxDepth. These rating curves are useful because they represent non-linear relationships between lake area (which we measure via Remote Sensing) and variables that we do not, i.e., depth (and with that elevation) and volume. These in turn are helpful to compute rates of volume change that we can relate to other processes in the hydrologic budget such as precipitation, evaporation, and evapotranspiration. We created these rating curves using standard GIS tools that would "fill the bathtub" to a pre-specified level and then computed area and volume based on appropriate tools from the GIS tool box. These rating curves as shown in Figures 21 and 22. Here we plot our three remaining parameters (volume, depth, elevation) versus our primary variable, i.e., lake area extent.

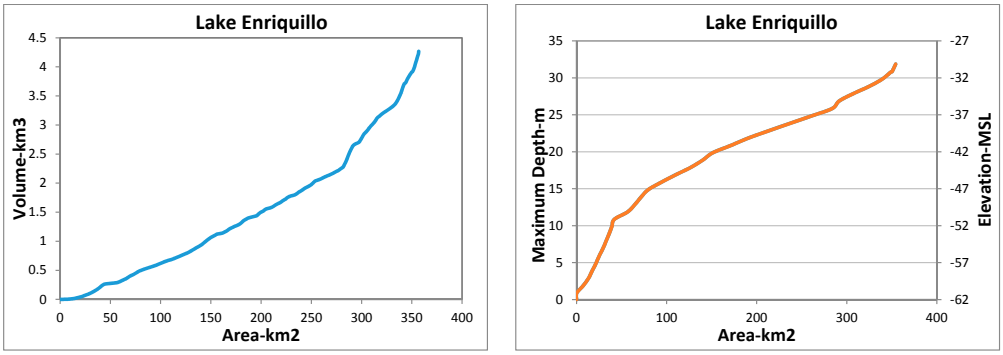

(**a**) (**b**)

Figure 21. (**a**) Lake Enriquillo volume-area rating curve; (**b**) Lake Enriquillo max depth/elevation-area rating curve.

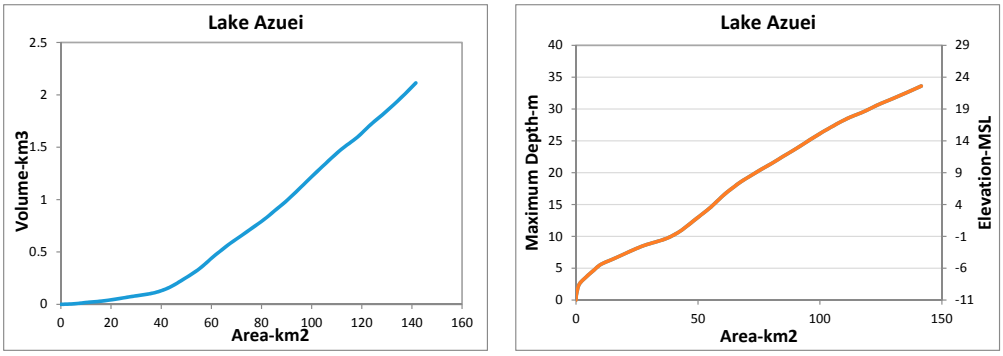

(**a**) (**b**)

Figure 22. (**a**) Lake Azuei volume-area rating curve; (**b**) Lake Azuei max depth/elevation-area rating curve.

Having constructed these rating curves, we are able to retrieve the volume of each lake for a specific date and time for a new value in the lake's surface area time series thus allowing us to quantify the volumetric changes of lakes at any time in the past, now, and most importantly in the future.

4. Discussion

4.1. Lake Volumes

The various efforts to collect data on the lakes over time has produced a small pool of sources that allows us to examine some of the previous work and compare it with our most recent efforts. In 2003, Schubert [19] published average values for Lake Enriquillo's volume ranging from 0.5 km^3 to 1.5 km^3 between the years of 1979 to 2002. Wright et al. [13] on the other side show a volume value range between 0.8 km^3 to 1.6 km^3 for the years from 1983 and 2002 while our work suggests a range between 1.2 km^3 to 2.1 km^3 for the same year span. For the years after 2002, the values of Wright et al. [13] and ours come closer, i.e., to about 3.8 km^3 in mid-2013. Although the volume's trend in all publications is much the same, many gaps can be seen in Schubert's [19] and Wright et al. [13] studies showing sudden volume oscillations before the years of 2001 which is unrealistic, since no such change has been shown in the corresponding surface area trend they presented, in addition to not having been reported by any other references.

Araguás-Araguás et al. [17] reported Lake Enriquillo's volume to be 1.7 km^3, however, no corresponding date was offered, rendering this information unusable. In 2012, Logan et al. [12] used the average surface area of the lake during the last decade (~250 km^2) and multiplied it by the depth

increase of the lake reported by INDRHI (~6 m since 2000) to calculate the volume change of the lake resulting in a 1.5 km^3 increase. Using the average volume in 2000 and considering 2011 as the target year, we compute a 5.9-m rise and a corresponding 1.6 km^3 increase in volume, i.e., reasonably close. They also compute a lake surface area growth of 0.16 km^3 from 20 July to 28 September 2011 when the lake purportedly rose by 0.5 m (reported by INDRHI). The images from those dates were not available, so we took the values for 12 July and 10 October. Our calculations show that the lake rose only by 0.2 m and thus only added 0.066 km^3 in volume. Unfortunately, these are the only other references that reported lake volume calculations producing numbers that we cannot confirm. We must assume that these differences result from the method and bathymetry map used to extract volume.

4.2. Lake Elevations

We discovered some references that report elevation values of Lake Enriquillo, while none were found for Lake Azuei. We have summarized the references in Table 8 listing the time frame for when the data points were collected, the number of data points, and the range of lake levels reported. Note that many of these references referenced other publications as the basis for their lake level estimation. For example, in 2009, Quezada [50] presented 12 different references for 14 elevation values and in 2013, Quezada [51] lists references for 32 elevation values. In 2003, Schubert [19] showed two different time series for elevation, however, without stating the reference. The other elevation time series in Table 8 are presented by UASD, INDRHI, PUND, and Wright et al. which are assumed to be generated by the researchers [10,11,13,49,52]. Unfortunately, neither reference stated how these values were extracted nor what the reference datum was to which the elevations were referenced, which is the major impediment for comparing lake levels.

Table 8. Lake Enriquillo elevation references.

Source	Timespan	Number of Data Points	Range of Values (m)
UASD [11,52]	1961–2011	11	−45.7 to −27.7
Quezada, 2013 [51]	1893–2009	31	−46.42 to +0.63
Quezada, 2009 [18,50,51]	1892–2009	14	−45.7 to +0.63
Schubert, 2003 [19]	1992–1999	14	−45.6 to −42.2 *
Schubert, 2003 [19]	1994–1995	5	−42.92 to −42.54 *
INDRHI [10,49]	1949–2002	27	−46.4 to −30.02
PNUD [52]	2000–2012	3	−43.7 to −30
Wright et al., 2015 [13]	1984–2013	57	−53.8 to −41.1 *

* The data is retrieved from the graph presented by the reference and the values are approximate.

Figure 23 (Lake Enriquillo) and Figure 24 (Lake Azuei) show a collection of time series plots from various literature sources, referenced to mean sea level, MSL. Since the DEM itself has an absolute vertical accuracy of 7 to 9 m for North America which contains Hispaniola as well [57], we decided to envelop our time series with an average band of ±4 m to reflect this uncertainty. Most of the graphing-values shown in Figure 23 are related to years before 2004 and there are just a few values produced for subsequent years. While most of the time series are close to each other, follow about the same trend, and fall into the grey band of uncertainty, it is also evident that the one derived from the Wright et al. study [13] and our study both of which have the highest point density, are set apart by about 5 m.

In an attempt to find an explanation for this significant difference, we examined the elevation data available in Google Earth and tried to match it to the DEM, which is referenced to the Earth Gravitational Model of 1996, EGM96. Constructing contour lines and then overlaying these with the DEM showed only negligible differences. A second thought concerned the potential use of GPS readings which are horizontally and vertically referenced to the WGS84 ellipsoid. Since the difference between the "static" ellipsoid and the undulating EGM96 geoid varies considerably as one moves across the globe, we sought to establish this difference for our location at the lakes, which is about 27 m.

Clearly, this difference is quite significant and much larger than the 5 m mentioned, thus rendering our thought-of-explanation invalid. Unfortunately, there is no tool available to our knowledge to validate the DEM elevations in addition to having no information about the error distribution, which in all likelihood is uneven for a given region. As mentioned before, having only a single GCP for the region, while helpful, would not be enough to correct/validate all elevation values of the DEM around the lakes, thus leaving any reference made to lake levels referenced to MSL with some degree of uncertainty.

The lakes' physical properties (except for MSL referenced elevations) can be calculated fairly accurately, however, based on the bathymetry, for those cases when the surface area polygon falls inside the bathymetry boundaries, i.e., below the shoreline polygon that was recorded in 2013. While the lakes were both at a fairly high state in 2013 this would cover any level below that line and only be fraught with uncertainty when we consider continued future lake growth which would reach elevations derived from the DEM rather than the collected bathymetry data, i.e., is above the "stitch-line".

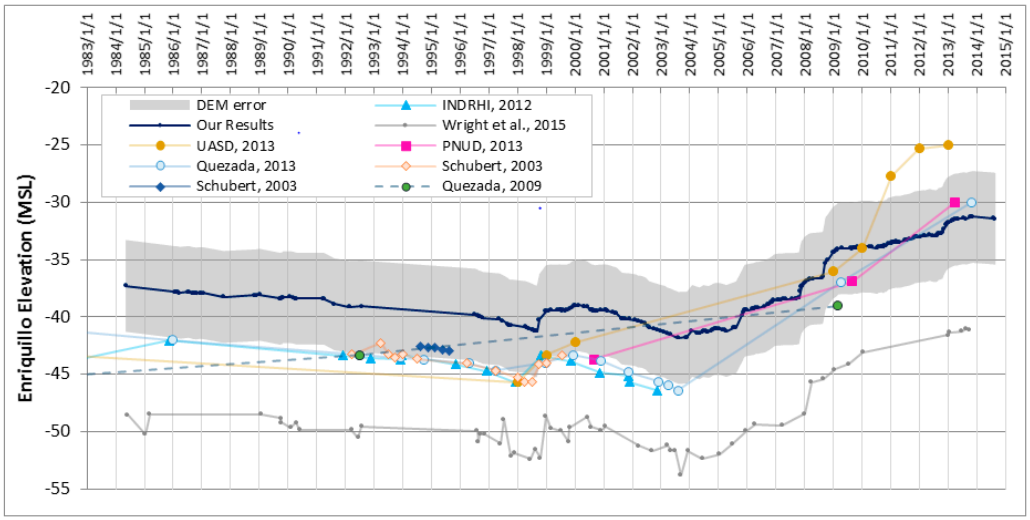

Figure 23. Lake Enriquillo elevation time series comparison.

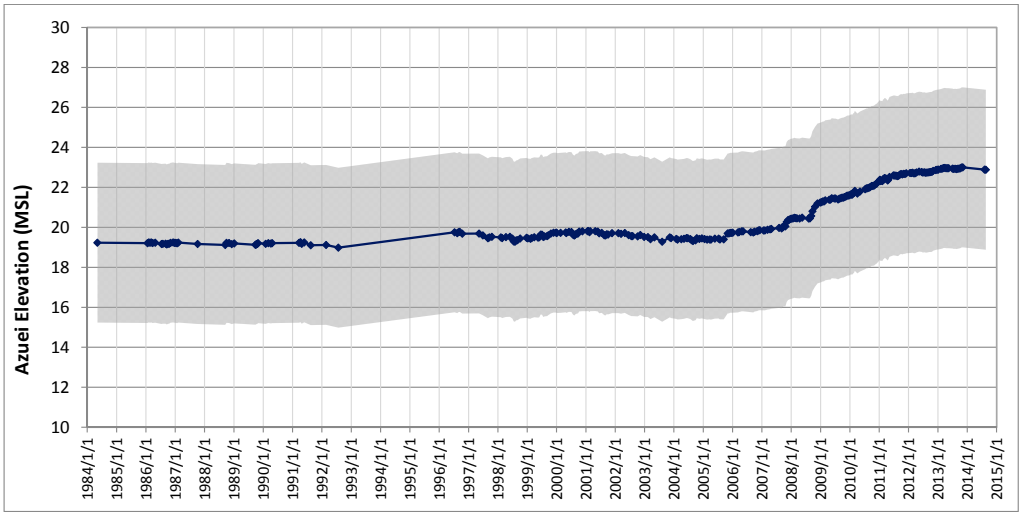

Figure 24. Lake Azuei elevation time series.

Our analysis shows that in summer of 1984 Lake Enriquillo's area and volume were 257.648 km^2 and 2.060 km^3, respectively. Then it started to shrink to 170.010 km^2 and 1.225 km^3 in summer of

1998 where it stayed relatively unchanged only to grow back again to 218.606 km^2 and 1.662 km^3 in late 2000. The second recession of the lake happened in 2003 when the lake area and volume were 157.952 km^2 and 1.131 km^3, respectively. Expanding over the next 10 years by the summer of 2013 the lake experienced it its biggest extent of record, i.e., 348.778 km^2, with an equivalent volume of 3.881 km^3. The last image we analyzed was for 21 August 2014 showing that the lake had arrested its expansion and actually receded somewhat to 346.694 km^2 and 3.823 km^3. The changes of Lake Azuei were less pronounced than for Lake Enriquillo even though both lakes experienced the same congruent recession growth patterns. In summer of 1984, Lake Azuei had a surface area of 115.002 km^2 and a volume of 1.531 km^3. After a period of moderate growth and recession, the lake reached its second low point late summer of 2003 when its size was 115.419 km^2 and 1.536 km^3 roughly the size it had in 1984. Like Lake Enriquillo, Lake Azuei grew substantially over the next 10 years to reach its maximum extent of 138.298 km^2 and 2.005 km^3 (Volume) by late 2013. Since then it largely maintained its levels even though the last analyzed image suggests that the lake has shrunk to 137.277 km^2 and 1.988 km^3. Note that the volumetric changes are quite different; from 2003 to 2013, Lake Enriquillo grew by 88% while Lake Azuei only added 31%. It is these differences that despite the close proximity of the lakes, prompt further research questions, i.e., why have they experienced such different growth values.

4.3. Future Lake Expansion

While the consequences of the lake expansion have been dramatic already in terms of loss of arable land, roads, and housing, even greater concern has been expressed for what would happen if the lakes were to continue to rise and expand; for example if at some point Lake Azuei would start overflowing and convey water directly to Lake Enriquillo through the Jimani depression. Since our bathtub model permits seamless "fill" and "drain" we examined what the consequences of future growth would be in terms of a) additional flooding and b) movement of water volumes. The results show that both lakes may continue to expand toward the shallow areas in the eastern and western expands of the lakes thus inundating significant additional swaths of arable land all the way to the point where they reach the lowest point in their watershed line. At this point, they would overflow and convey water to neighboring watersheds. Lake Azuei will reach this "overflow" point at a maximum area extent of 154.58 km^2 (and an approximate MSL of 28 m) on its western shores, while Lake Enriquillo passes its watershed border on the east side when its surface area is 860.86 km^2 (and an approximate MSL of 13 m). Figure 25 shows the maximum extent of each lake for the given maximum elevation.

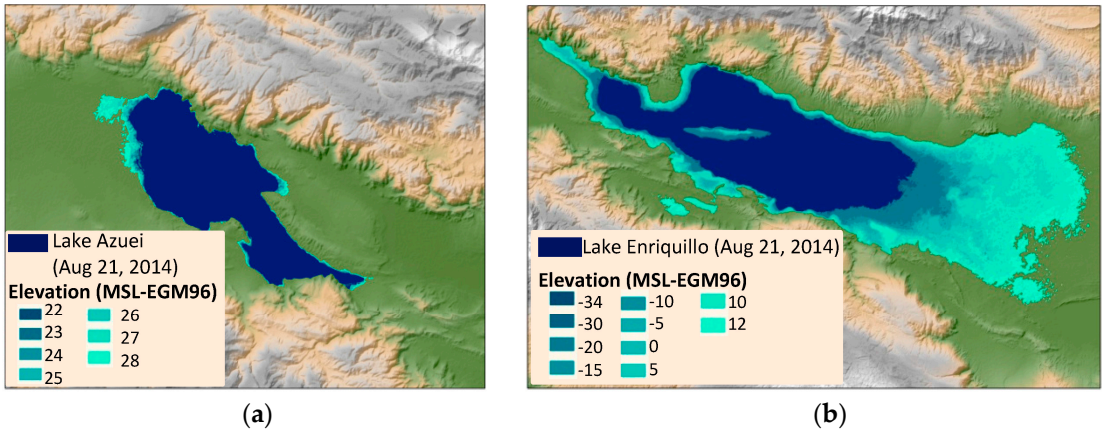

Figure 25. (**a**) Lake Azuei growth pattern; (**b**) Lake Enriquillo growth pattern.

It is worthwhile to examine the longitudinal cross section (about E–W) of the rift valley (as shown in Figure 26), i.e., from the Bay of Port-au-Prince in the west to the Bay of Neiba in the east, which would be the ultimate drainage points. Lake Azuei would drain to the west by first spilling over into

the much smaller Lake Caiman (which sits at a higher elevation, with 4.7 km^2 surface area) and fill the Caiman basin until the lowest point in the basin boundary has been reached and then convey water through the Boucan Brou Canal connecting its basin to the Bay of Gonaves at Port-au-Prince. As a consequence, Lake Azuei will never rise higher than ~28 m MSL and also never flood and spill through the Jimani depression. Lake Enriquillo on the other hand, being so low, would need to rise to about +13 m MSL, another 40+ m from its current levels to spill out on its eastern shore first into the Lake Rincon basin (36.38 km^2 surface area) and then into the Yaque del Sud en route to the Caribbean at Barahona. This maximum or "spill" level is depicted in Figure 27 with the completely flooded Caiman and Rincon added to the image composition.

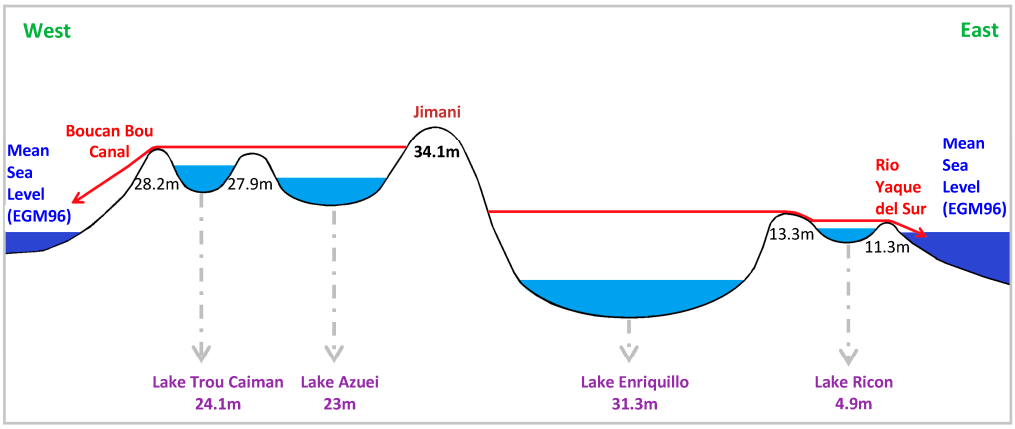

Figure 26. Schematic vertical topographic profile of lakes.

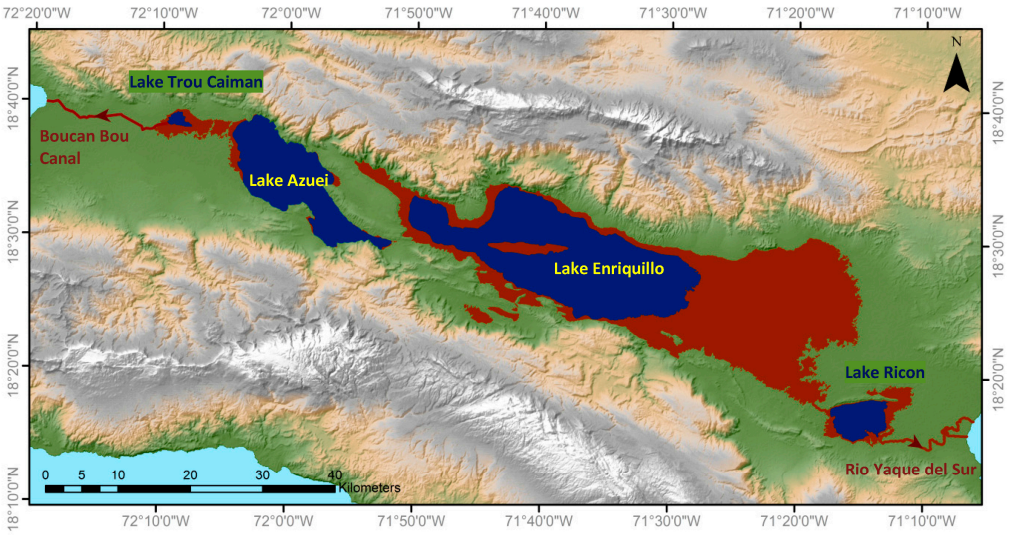

Figure 27. Trou-Caiman, Azuei, Enriquillo, and Ricon Lake growth.

Although it is clear that Lake Azuei will not overflow into Lake Enriquillo, both lakes will expand towards each other and cause flooding in parts of Jimani and the surrounding town lands. We used the topographic information we have for Jimani to identify which areas of the town and its surrounding environment would be subject to flooding considering the maximum extent of both lakes. The results of overlaying the maximum flood line of each lake with a Google Earth map is shown in Figure 28. Although the elevation data in Google Earth is slightly different from the DEM, the differences are small enough to give a fairly accurate inundation line for the western and eastern reaches of Jimani. While the lakes would come to within about 500 m of each other they would not connect and most

of Jimani would not be affected because it lies at slightly higher elevations than the lowest point in the divide. Note though that this is a purely hypothetical consideration and while Lake Azuei is only about 5 m away from its high point (Lake Enriquillo is about 40–50 m away) recent trends suggest that the lake's growth has stopped at about their current state (as mentioned before actually slightly less).

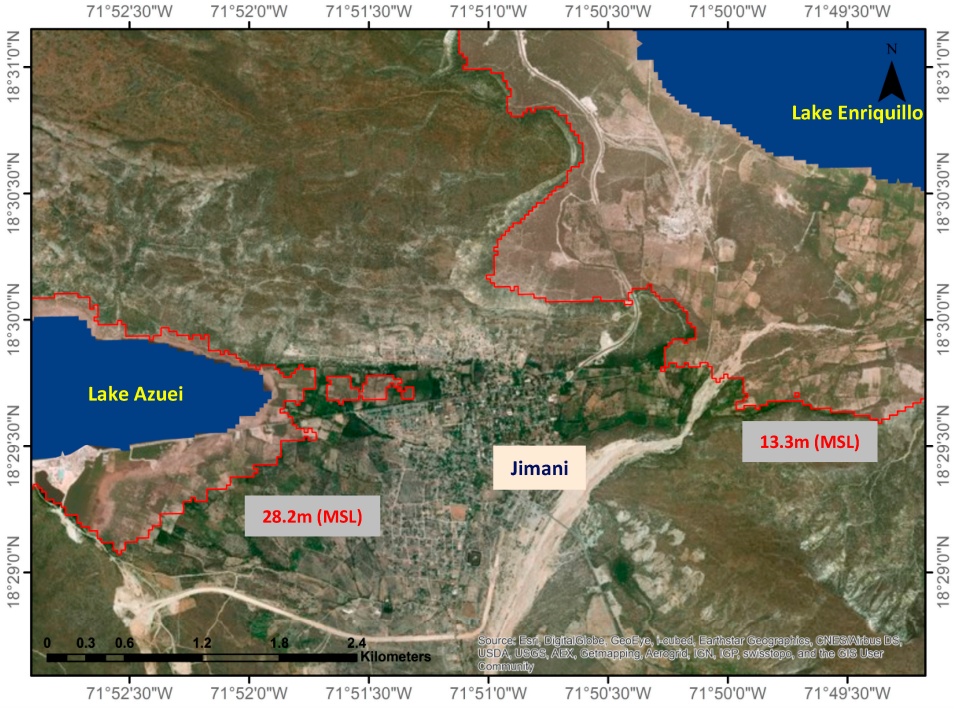

Figure 28. Flood map of Jimani in case of maximum lakes' extension.

5. Conclusions

In this case study, we used remote sensing methods to construct lake extent time series and subsequent rating curves of depth and volume for Lakes Azuei and Enriquillo in the Hispaniola rift valley. We used a pool of almost 300 images for which we also applied remote sensing and gap filling techniques to give us the ability to distinguish water bodies from cloud and cloud shadows and make use of most of the images that did not have acceptable quality before, to draw information from. We compiled the densest and completest time series of the surface area for the two lakes to date showing a lot more temporal detail, which can be used to shed some light on seasonal and even monthly timescale hydro-meteorological processes.

In order to derive volume, depth, and elevation information, we combined the bathymetry of the lakes with an existing high resolution (30 m) DEM and created a "bath-tub" model for the study area. We examined the issues that arrive when trying to "stitch" two different elevation data sets (each derived with entirely different means) together. We suggested some solutions and also stressed the importance of needing a set of Geographic Control Points (GCPs) that establish proper vertical datum references.

We demonstrated how the surface area values from the Landsat images serve as input information to obtain volume, depth, and elevation data out of rating curves which in turn are required information for investigating the water balance of the lakes. We also used our model to examine and answer questions such as: Will Lake Azuei spill over into Lake Enriquillo? (it will not); what are the maximum attainable lake levels and what impact would result if the lakes were to reach these maximum levels? (Lake Azuei would flow over into the Bay of PaP and Lake Enriquillo would spill over and empty towards the Bay at Barohuco); Will Jimani eventually get flooded (it will not, even though some low-lying town areas may be impacted).

Acknowledgments: We would like to acknowledge the National Science Foundation who supported this work with Award numbers: 1264466 and 1513512. We would also like to extend our gratitude to Fred Moshary and Daniel Comarazamy of the City College of New York and NOAA, respectively for their valuable input especially early in the project when carrying out the first steps of this research. This work has received some support from CCNY students that worked on this topic via Senior Projects, as a class project in the Introduction to GIS course, or as an independent study for which we are thankful. Lastly, we are grateful to Paul Mann of the University of Houston for his continued support and insight as well as sharing sonar data sets that complemented ours.

Author Contributions: The first author, Mahrokh Moknatian, is the primary individual who carried out all the tasks and steps that are presented in this manuscript. Michael Piasecki, the second author and advisor, contributed to the ideas and task components (design) that needed to be carried out to arrive at the results presented. He is also a significant contributor to the writing/editing effort of this manuscript. Jorge Gonzalez has significantly contributed being the Lead PI of the project that originally funded the first steps of this research in addition to having added to the discussion on how to proceed and interpret the results. In this latter activity, he has been instrumental as he is leading the Hydro Climatology research component that accompanies the work done by the lead author. All three authors have been to the Lakes area on several field trips collecting the required data that is in part presented in this manuscript.

Conflicts of Interest: The authors declare no conflict of interest.

References

1. UN News Service. Haiti and Dominican Republic Partner to Save Border Lakes with UN's Help. 2009. Available online: www.UN.org (accessed on 16 September 2009).
2. The Guardian. Rapidly Rising Lake Levels Threaten Trade on Dominican-Haiti Border. 2012. Available online: www.TheGuardian.com (accessed on 31 August 2012).
3. Archibold, R.C. Rising Tide Is a Mystery That Sinks Island Hopes. 2014. Available online: www.NYTimes.com (accessed on 11 January 2014).
4. Arroyo, L. "El Agua se lo Llevó Todo": El Misterio de Los Lagos Crecientes del Caribe. 2014. Available online: www.BBC.com (accessed on 16 January 2014).
5. Europa Press. El Lago del Caribe que Crece de Forma Inexplicable. 2014. Available online: www.ABC.es (accessed on 16 January 2014).
6. Vice News. The Lake That Burned Down a Forest (Lake Enriquillo, Dominican Republic). 2014. Available online: www.News.Vice.com (accessed on 27 July 2014).
7. Kushner, J. The Relentless Rise of Two Caribbean Lakes Baffles Scientists. 2016. Available online: www.Nationalgeographic.com (accessed on 3 March 2016).
8. Earth & Space Science News. Climate Change's Pulse Is in Central America and the Caribbean. 2017. Available online: www.EOS.org (accessed on 27 April 2017).
9. Perrissol, M.; Lescoulier, C. *Etude Hydrologique et Hydrogéologique de la Montée des Eaux du Lac Azueï*; Rapport de Mission, Version 2; Egis International: Haiti, 2011.
10. Buck, D.; Brenner, M. Physical and chemical properties of hypersaline Lago Enriquillo, Dominican Republic. *Int. Ver. Theor. Angew. Limnol. Verh.* **2005**, *29*, 725–731.
11. Méndez-tejeda, R.; Rosado, G.; Rivas, D.V.; Montilla, T.; Hernández, S.; Ortiz, A.; Santos, F. Climate variability and its effects on the increased level of Lake Enriquillo in the Dominican Republic, 2000–2013. *Appl. Ecol. Environ. Sci.* **2016**, *4*, 26–36.
12. Logan, W.S.; Enfield, D.B.; Division, P.O.; Capdevila, A.S. Rising Water Levels at Lake Enriquillo, Dominican Republic: Advice on Potential Causes and Pathways forward. Report by the International Center for Integrated Water Resources Management (ICIWaRM) to the Instituto Nacional de Recursos Hidráulicos (INDRHI), Government of the Dominican Republic. 2012. Available online: https://s3.amazonaws.com/sitesusa/wp-content/uploads/sites/422/2015/12/Lake_Enriquillo_report_1-26-2012.pdf (accessed on 9 December 2015).
13. Wright, V.D.; Hornbach, M.J.; Mchugh, C.; Mann, P. Factors contributing to the 2005-present, rapid rise in lake levels, Dominican Republic and Haiti (Hispaniola). *Nat. Resour.* **2015**, *6*, 465–481. [CrossRef]
14. Luna, E.J.R.; Poteau, D. Water Level Fluctuations of Lake Enriquillo and Lake Saumatre in Response to Environmental Changes. Master's Thesis, Cornell University, Ithaca, NY, USA, 2011.
15. Fortun, J. *Environmental Impacts on Lake Azueï in Haiti due to Degradation of Its Watersheds*; University of Puerto Rico: San Juan, Puerto Rico, 2011.

16. Comarazamy, D.E.; González, J.E.; Moshary, F.; Piasecki, M. On the hydrometeorological changes of a tropical water basin in the Caribbean and its sensitivity to midterm changes in regional climate. *J. Hydrometeorol.* **2015**, *16*, 997–1013. [CrossRef]
17. Araguás Araguás, L.; Mchelen, C.; Garcia, A.; Medina, J.; Febrillet, J. *Estudio de la Dinamica del Lago Enriquillo: Segundo Informe de Avance*; Project DOM/8/006; International Atomic Energy Agency: Vienna, Austria, 1995.
18. Pichardo, F.D.G.; Conte, L.L.; Regio, G. *Alternativas Productivas a Mediano y Largo Plazo Para las Familias Afectadas por la Crecida del Nivel del Lago Enriquillo*; Study Report; OXFAM, FAO y Comisión Europea: Santo Domingo, Dominican Republic, 2012.
19. Schubert, A. *El Lago Enriquillo—Gran Patrimonio Natural y Cultural del Caribe*, 2nd ed.; Secretaría de Medio Ambiente y Recursos Naturales Consorcio Ambiental Dominicano CAD: Jimaní, Dominican Republic, 2003.
20. Piasecki, M.; Moknatian, M.; Moshary, F.; Cleto, J.; Leon, Y.; Gonzalez, J.; Comarazamy, D. Development of geospatial lake representations: Hispaniola's Lake Azuei and Enriquillo. *Caribb. J. Sci.* **2015**, accepted.
21. González, R.; Brito, D.R.; González, J. *Estudio Hidrogeológico de la Zona del Lago Enriquillo, Determinación de las Causas del Aumento de Nivel de sus Aguas e Intervenciones Requeridas para su Control*; Informe No. 1 de Avance del Proyecto; INTEC/CCNY, 2010.
22. Fritz, S.C.; Cumming, B.F.; Gasse, F.; Laird, K.R. Diatoms as indicators of hydrologic and climatic change in saline lakes. In *The Diatoms: Applications for the Environmental and Earth Sciences*; Stoermer, E.F., Smol, J.P., Eds.; Cambridge University Press: Cambridge, UK, 2001; Volume 102, pp. 186–208.
23. Maiersperger, T.K.; Scaramuzza, P.L.; Leigh, L.; Shrestha, S.; Gallo, K.P.; Jenkerson, C.B.; Dwyer, J.L. Characterizing LEDAPS surface reflectance products by comparisons with AERONET, field spectrometer, and MODIS data. *Remote Sens. Environ.* **2013**, *136*, 1–13. [CrossRef]
24. Chávez, P.S.J. Image-Based Atmospheric Corrections—Revisited and Improved. *Photogramm. Eng. Remote Sens.* **1996**, *62*, 1025–1036.
25. Martinuzzi, S.; Gould, W.; González, O. *Creating Cloud-Free Landsat ETM+ Data Sets in Tropical Landscapes: Cloud and Cloud-Shadow Removal*; General Technical Report IITF-GTR-32; International Institute of Tropical Forestry: Ro Piedras, Puerto Rico, 2007.
26. Jedlovec, G. Automated Detection of Clouds in Satellite Imagery. Advances in Geoscience and Remote Sensing, 2009. Available online: https://www.intechopen.com/books/advances-in-geoscience-and-remote-sensing/automated-detection-of-clouds-in-satellite-imagery (accessed on 22 May 2017).
27. Irish, R.R. Landsat 7 automatic cloud cover assessment. *AeroSense* **2000**, *4049*, 348–355.
28. Huang, C.; Thomas, N.; Goward, S.N.; Masek, J.G.; Zhu, Z.; Townshend, J.R.G.; Vogelmann, J.E. Automated masking of cloud and cloud shadow for forest change analysis using Landsat images. *Int. J. Remote Sens.* **2010**, *31*, 5449–5464. [CrossRef]
29. Hughes, M.; Hayes, D. Automated detection of cloud and cloud shadow in single-date Landsat imagery using neural networks and spatial post-processing. *Remote Sens.* **2014**, *6*, 4907–4926. [CrossRef]
30. Irish, R.R.; Barker, J.L.; Goward, S.N.; Arvidson, T. Characterization of the Landsat-7 ETM+ Automated Cloud-Cover Assessment (ACCA) Algorithm. *Photogramm. Eng. Remote Sens.* **2006**, *72*, 1179–1188. [CrossRef]
31. Zhu, Z.; Wang, S.; Woodcock, C.E. Improvement and expansion of the Fmask algorithm: Cloud, cloud shadow, and snow detection for Landsats 4-7, 8, and Sentinel 2 images. *Remote Sens. Environ.* **2015**, *159*, 269–277. [CrossRef]
32. Zhu, Z.; Woodcock, C.E. Object-based cloud and cloud shadow detection in Landsat imagery. *Remote Sens. Environ.* **2012**, *118*, 83–94. [CrossRef]
33. Helmer, E.H.; Ruefenacht, B. Cloud-free satellite image mosaics with regression trees and histrogram matching. *Photogramm. Eng. Remote Sens.* **2005**, *71*, 1079–1089. [CrossRef]
34. Wang, B.; Ono, A.; Muramatsu, K.; Fujiwara, N. Automated detection and removal of clouds and their shadows from Landsat TM images. *IEICE Trans. Inf. Syst.* **1999**, *82*, 453–460.
35. Jin, S.; Homer, C.; Yang, L.; Xian, G.; Fry, J.; Danielson, P.; Townsend, P.A. Automated cloud and shadow detection and filling using two-date Landsat imagery in the USA. *Int. J. Remote Sens.* **2013**, *34*, 1540–1560. [CrossRef]
36. Li, W.; Du, Z.; Ling, F.; Zhou, D.; Wang, H.; Gui, Y.; Sun, B.; Zhang, X. A comparison of land surface water mapping using the Normalized Difference Water Index from TM, ETM+ and ALI. *Remote Sens.* **2013**, *5*, 5530–5549. [CrossRef]

37. Li, M.; Xu, L.; Tang, M. An extraction method for water body of remote sensing image based on oscillatory network. *J. Multimed.* **2011**, *6*, 252–260. [CrossRef]
38. Xu, H. Modification of normalised difference water index (NDWI) to enhance open water features in remotely sensed imagery. *Int. J. Remote Sens.* **2006**, *27*, 3025–3033. [CrossRef]
39. Jiang, H.; Feng, M.; Zhu, Y.; Lu, N.; Huang, J.; Xiao, T. An automated method for extracting rivers and lakes from Landsat Imagery. *Remote Sens.* **2014**, *6*, 5067–5089. [CrossRef]
40. McFeeters, S.K. Using the normalized difference water index (NDWI) within a geographic information system to detect swimming pools for mosquito abatement: A practical approach. *Remote Sens.* **2013**, *5*, 3544–3561. [CrossRef]
41. Wilson, E.H.; Sader, S.A. Detection of forest harvest type using multiple dates of Landsat TM imagery. *Remote Sens. Environ.* **2002**, *80*, 385–396. [CrossRef]
42. Shen, L.; Li, C. Water body extraction from Landsat ETM+ imagery using adaboost algorithm. In Proceedings of the 18th International Conference on Geoinformatics, Beijing, China, 18–20 June 2010; pp. 3–6.
43. Daniels, R.C. Using ArcMap to extract shorelines from Landsat TM & ETM+ data. In Proceedings of the Thirty-Second ESRI International Users Conference, San Diego, CA, USA, 12–16 July 2010; pp. 1–23.
44. Feyisa, G.L.; Meilby, H.; Fensholt, R.; Proud, S.R. Automated Water Extraction Index: A new technique for surface water mapping using Landsat imagery. *Remote Sens. Environ.* **2014**, *140*, 23–35. [CrossRef]
45. Ji, L.; Zhang, L.; Wylie, B. Analysis of dynamic thresholds for the Normalized Difference Water Index. *Photogramm. Eng. Remote Sens.* **2009**, *75*, 1307–1317. [CrossRef]
46. Chen, J.; Zhu, X.; Vogelmann, J.E.; Gao, F.; Jin, S. A simple and effective method for filling gaps in Landsat ETM+ SLC-off images. *Remote Sens. Environ.* **2011**, *115*, 1053–1064. [CrossRef]
47. Zhang, C.; Li, W.; Travis, D. Gaps-fill of SLC-off Landsat ETM+ satellite image using a geostatistical approach. *Int. J. Remote Sens.* **2007**, *28*, 5103–5122. [CrossRef]
48. Afshari, S. sha17hab/Flood-Inundation-Mapping-and-Comparison-of-Two-Models: Flood-Inundation-Mapping-and-Comparison-of-Two-Models. *Zenodo* **2016**. [CrossRef]
49. Schubert, A. *Lagos Enriquillo y Azuéi. Donde la Naturaleza Siempre Tiene Una Sorpresa*; Editorial Académica Española, Ed.; LAP Lambert Academic Publishing GmbH & Co. KG: Saarbrücken, Germany, 2012.
50. Quezada, A.C. El Ciclo Hidrologico del Lago Enriquillo y la Crecida Extrema del, 2009. Available online: http://www.acqweather.com/EL%20CICLO%20HIDROLOGICO%20DEL%20LAGO%20ENRIQUILLO.pdf (accessed on 16 April 2009).
51. Quezada, A.C. La Oscilacion Natural del Lago Enriquillo (ONLE): Un Evento Hidrometeorológico que Responde a la Variabilidad Climática de la República Dominicana. Available online: http://www.acqweather.com/LA%20ONLE%20Final.pdf (accessed on 24 December 2013).
52. Programa de Naciones Unidas para el Desarrollo (PNUD). *Plan Estratégico de Recuperación y Transición al Desarrollo para la Zona del Lago Enriquillo*; Editora Búho, Proyecto Frontera—UNDP: Santo Domingo, Dominican Republic, 2013.
53. The Hispaniola Lakes Project. Available online: http://cuerg.ccny.cuny.edu/hispaniola (accessed on 30 December 2016).
54. CATHALAC. Expansion of Haiti's Lake Azuei. Available online: http://www.un-spider.org/news-and-events/news/cathalac-subsequent-analysis-lake-azuei-flooding (accessed on 2 October 2012).
55. Buck, D.G. Limnology and Paleolimnology of Hypersaline Lago Enriquillo, Dominican Republic. Master's Thesis, University of Florida, Gainesville, FL, USA, 2004.
56. INTEC (Instituto Tecnológico de Santo Domingo). Científicos Completan el Mapa de Fondo de los Lagos Enriquillo y Azuéi. Available online: http://www.intec.edu.do/noticias-y-actividades/noticias/item/cientificos-completan-el-mapa-de-fondo-de-los-lagos-enriquillo-y-azuei (accessed on 12 September 2013).
57. Rodriguez, E.; Morris, C.S.; Belz, J.E.; Chapin, E.C.; Martin, J.M.; Daffer, W.; Hensley, S. *An Assessment of the SRTM Topographic Products*; Technical Report JPL; Jet Propulsion Laboratory: Pasadena, CA, USA, 2005.